Processes controlling the annual cycle of Arctic aerosol number and size distributions

B. Croft[1], R. V. Martin[1,2], W. R. Leaitch[3], P. Tunved[4], T. J. Breider[5], S. D. D'Andrea[6], and J. R. Pierce[6,1]

[1]{Department of Physics and Atmospheric Science, Dalhousie University, Halifax, NS, Canada}
[2]{Harvard-Smithsonian Center for Astrophysics, Cambridge, MA, USA}
[3]{Science and Technology Branch, Environment Canada, Toronto, Ontario, Canada}
[4]{Department of Environmental Science and Analytical Chemistry, Stockholm University, Stockholm, Sweden}
[5]{School of Engineering and Applied Sciences, Harvard University, Cambridge, MA, USA}
[6]{Department of Atmospheric Science, Colorado State University, Fort Collins, CO, USA}

Correspondence to: B. Croft (bcarlin@dal.ca)

Abstract

Measurements at high-Arctic sites (Alert, Nunavut and Mt. Zeppelin, Svalbard) during the years 2011 to 2013 show a strong and similar, annual cycle in aerosol number and size distributions. Each year at both sites, the number of aerosols with diameters larger than 20 nm exhibits a minimum in October, and two maxima, one in spring associated with a dominant accumulation mode (particles 100 nm to 500 nm in diameter), and a second in summer associated with a dominant Aitken mode (particles 20 nm to 100 nm in diameter). Seasonal-mean aerosol effective diameter from measurements ranges from about 180 nm in summer to 260 nm in winter. This study interprets these annual cycles with the GEOS-Chem-TOMAS global aerosol microphysics model. Important roles are documented for several processes (new-particle formation, coagulation scavenging in

clouds, scavenging by precipitation, and transport) in controlling the annual cycle in Arctic aerosol number and size.

Our simulations suggest that coagulation scavenging of interstitial aerosols in clouds by aerosols that have activated to form cloud droplets strongly limits the total number of particles with diameters less than 200 nm throughout the year. We find that the minimum in total particle number in October can be explained by diminishing new-particle formation within the Arctic, limited transport of pollution from lower latitudes, and efficient wet removal. Our simulations indicate that the summertime-dominant Aitken mode is associated with efficient wet removal of accumulation-mode aerosols, which limits the condensation sink for condensable vapours. This in turn promotes new-particle formation and growth. The dominant accumulation mode during spring is associated with build up of transported pollution from outside the Arctic coupled with less-efficient wet removal processes at colder temperatures. We recommend further attention to the key processes of new-particle formation, interstitial coagulation, and wet removal and their delicate interactions and balance in size-resolved aerosol simulations of the Arctic to reduce uncertainties in estimates of aerosol radiative effects on the Arctic climate.

1. Introduction

The climate impact of aerosols strongly depends on aerosol number and size distributions (Haywood and Boucher, 2000; Lohmann and Feichter, 2005). These aerosol properties, in addition to chemical composition, contribute to aerosol effects on the Earth's climate. Aerosols influence the global climate directly through scattering and absorption of radiation (Charlson et al., 1992), and indirectly by modifying cloud properties

(Twomey, 1974; Albrecht, 1989). Aerosols play an important role in the Arctic climate, and changing aerosol concentrations are believed to have contributed to the rapid Arctic warming observed over the past few decades (Shindell and Faluvegi, 2009). However, in the Arctic there are complex aerosol feedbacks and strong seasonal aerosol cycles that make study of aerosol-climate interactions particularly challenging in this remote region (Browse et al., 2012; 2015). To address a portion of this challenging puzzle, this study focuses on understanding the processes that control the Arctic aerosol number and size distributions over the entire annual cycle.

Observations at Arctic sites show a strong and similar annual cycle in aerosol number and size distributions (e.g. Ström et al., 2003; Leaitch et al., 2013; Tunved et al., 2013). In the high Arctic, at Mt. Zeppelin, Svalbard, and Alert, Nunavut, Canada, the observed annual cycle in aerosol number exhibits two maxima: one in March-April associated with dominance of accumulation-mode particles and one in July associated with smaller, Aitken-mode particles. The inter-seasonal transition from accumulation-mode-dominated springtime distributions to Aitken-mode-dominated summertime distributions has been observed not only at surface sites, but also in the free troposphere (Engvall et al., 2008). This inter-seasonal transition from spring to summer has been extensively studied; evidence suggests control by changes in aerosol wet removal efficiency, new-particle formation, and transport patterns (e.g. Korhonen et al., 2008, Garrett et al., 2010, Sharma et al., 2013). More-efficient wet removal in the mid latitudes and within the Arctic in late spring and summer inhibits transport of aged accumulation-mode aerosols into the Arctic. These summertime conditions favour new-particle formation (hereafter referred to as

NPF) from precursor vapours within the Arctic boundary layer due to the low condensation sink for particle-precursor vapours on to existing aerosol surface area, and the low coagulation sink for newly formed, growing particles (Leaitch et al., 2013; Heintzenberg et al., 2015).

Korhonen et al. (2008) conducted a pioneering global aerosol model study to interpret the processes controlling the spring–to-summer transition in Arctic aerosol number and size observed from Svalbard and the shipboard campaigns of Heintzenberg et al. (2006). The focus of that study was limited to spring-summer and the transition between these seasons. In our study, we extend the temporal scope to consider the entire annual cycle and use observations from both Svalbard and Nunavut, about 1000 kilometers apart. Over recent years, numerous studies have focused on the spring-summer transitions in aerosol mass abundance using observations and models to examine the role of transport and scavenging (Garrett et al., 2010; Garrett et al., 2011; Browse et al., 2012; DiPierro et al., 2013; Sharma et al., 2013, Stohl et al., 2013). However, there has been considerably less focus on Arctic aerosol number and size distributions. To our knowledge, ours is the first global modeling study to consider the complete annual cycle in Arctic aerosol number and size.

In this study, we examine aerosol number and size distributions over recent years (2011-2013) at the Canadian high-Arctic measurement site at Alert, Nunavut (82.5 °N) and the European site at Mt. Zeppelin, Svalbard (79 °N). We use the GEOS-Chem global chemical transport model (Bey et al., 2001; www.geos-chem.org) with the size-resolved aerosol microphysics package TOMAS (D'Andrea et al., 2013; Pierce et al., 2013;

Trivitayanurak et al., 2008) to examine the relative importance of various aerosol processes (NPF, emissions, removal, and microphysical processes such as condensation and coagulation) in controlling the annual cycle of aerosol number and size distribution in the Arctic.

While the importance of wet removal is well known (Korhonen et al., 2008; Garrett et al., 2010; Browse et al., 2012), relatively less attention has been given to coagulation of interstitial particles in clouds, which is another sink process for aerosol number. We implemented a mechanism in GEOS-Chem-TOMAS that represents coagulation between aerosols that have activated to form cloud droplets and interstitial aerosols (defined as particles within clouds, but outside of cloud droplets). This mechanism accounts for the ~100-fold increase in size (due to water uptake) for particles that are cloud condensation nuclei (CCN) and have activated to form cloud droplets. This size change increases the coagulation rate of smaller Aitken-mode aerosols with these larger activated aerosols. Pierce et al. (2015) showed that the inclusion of this mechanism to GEOS-Chem-TOMAS brings aerosol size distributions to closer agreement with observations, globally. Cesana et al. (2012) analyzed CALIOP retrievals using the cloud-phase detection algorithm and found that low-level liquid clouds are ubiquitous in all seasons in the Arctic. Thus, this in-cloud coagulation process is particularly relevant for the Arctic.

The following section describes the 2011-2013 high-Arctic measurements and gives an overview of the GEOS-Chem-TOMAS simulations conducted for this study. Section 3 examines the monthly and seasonal mean in-situ observations of aerosol number and size from scanning mobility particle sizer (SMPS) at Alert, and differential mobility particle

sizer (DMPS) at Mt. Zeppelin. The GEOS-Chem-TOMAS model is used to interpret the annual cycle of these measurements. We subsequently present the process rates that control the aerosol annual cycles in our simulations.

2. Method

2.1. Measurements at Alert

Measurements of particle size distributions at Alert have been ongoing since March 2011 with the exception of a few technical interruptions. Sampling of the ambient aerosol size distribution at Alert was conducted as described by Leaitch et al. (2013). Briefly, the particles are sampled through stainless steel tubing with a mean residence time for a particle from outside to its measurement point of approximately 3 s. At the point of sampling, the aerosol is at a temperature (T) of approximately 293K and the relative humidity (RH) is <50%. The total number concentration of particles larger than 10 nm in diameter at Alert is measured with a TSI 3772 Condensation Particle Counter (CPC) operating at a flow rate of 1 litre min^{-1} (lpm). The size distributions for particles from 20 nm to 500 nm in diameter are measured with a TSI 3034 Scanning Mobility Particle System (SMPS), operating at a flow rate of 1 lpm and verified for sizing on site using mono-disperse particles of polystyrene latex and of ammonium sulphate generated with a Brechtel Manufacturing Incorporated (BMI) Scanning Electrical Mobility Spectrometer (SEMS) and for number concentrations through comparison with the TSI 3772 CPC. The Alert SMPS data are accurate to within 15%, in terms of number concentration and sizing. The TSI 3772 CPC was initially compared with a TSI 3775 CPC temporarily operating at the site and measuring the number of particles with sizes larger than 4 nm.

148 The differences between the TSI 3772 and 3775 CPC were found to be <10% when there
149 was no evidence of particles smaller than 10 nm. The TSI 3772 CPC also compares to
150 within 10% with the SMPS when particle sizes are large enough for all particles to be
151 counted by both instruments (e.g. during periods of Arctic Haze).

152

153 ## *2.2. Measurements at Mt. Zeppelin*

154 The Department of Environmental Science and Analytical Chemistry, Section for
155 Atmospheric research (ACES), Stockholm University (SU), has monitored the sub-
156 micron aerosol number size distribution at Mt. Zeppelin since 2000 with a differential
157 mobility particle sizer (DMPS). Today, this more-than-15-year continuous dataset
158 constitutes one of the longest unbroken aerosol number size distribution observation
159 series in the Arctic.

160

161 During the 15 years of operation, the DMPS system has undergone a number of
162 modernizations. Initially a single differential mobility analyzer (DMA) system was used
163 covering a size range between roughly 20-600 nm. A major overhaul was performed
164 during late 2010, and since then the setup has remained unchanged, covering a size range
165 of 5-800 nm. Thus, the data used in our study (2011-2013) come from the same
166 instrument configuration.

167

168 This DMPS-system utilizes a custom-built twin DMA setup comprising one Vienna-type
169 medium DMA coupled to a TSI CPC 3772 covering sizes between 25-800 nm and a
170 Vienna-type long DMA coupled with at TSI CPC 3772 effectively covering sizes

between 5-60 nm. The size distributions from the two systems are harmonized on a common size grid and then merged. Both systems use a closed-loop setup. The inlet hat is a whole air inlet according to EUSAAR standard. At current setup, the inlet operates with a flow rate of about 100 lpm and consists of several stainless steel tubes. The 25 mm diameter DMPS sampling tube is in total 4.5 m long. Inside the station, the flow is split into progressively smaller tubing until reaching 1 lpm at the DMPS. Laminar flow condition applies throughout the sampling line. On the outside, the inlet temperature is kept above 273K using active heating. Inside the station the temperature increases gradually to room temperature (maximum temperature of 298K, but typically around 293K). RH and T are internally monitored and measurements are at dry conditions with RH<30%. The system is regularly checked with latex spheres and flow controls. The data are manually screened and crosschecked with other available observations.

2.3. GEOS-Chem-TOMAS model description

In this study, we use the GEOS-Chem-TOMAS model, which couples the GEOS-Chem global chemical transport model (www.geos-chem.org, Bey et al., 2001) with the TwO-Moment Aerosol Sectional (TOMAS) microphysics scheme (Adams and Seinfeld, 2002; Lee and Adams, 2012). All simulations use GEOS-Chem version 9.02 at 4°x5° resolution globally, corresponding to 440 km x 95 km at 80 °N. The model has 47 layers extending from the surface to 0.01 hPa. Simulations at Mt. Zeppelin are sampled at the station altitude of 500 m. Assimilated meteorology is from the National Aeronautics and Space Administration (NASA) Global Modelling and Assimilation Office (GMAO) Goddard Earth Observing System version 5 (GEOS-5). All simulations use meteorology and emissions for the year 2011 following 3 months spin-up at the end of 2010. GEOS-

Chem includes simulation of more than 50 gas-phase species including oxidants such as OH and aerosol-precursor gases such as SO_2 and NH_3. Emissions in GEOS-Chem-TOMAS are described in Stevens and Pierce (2014). In addition, we implement seabird-colony NH_3 emissions from Riddick et al. (2012) with modifications for additional colonies in the Arctic region based on the on-line Circumpolar Seabird Data Portal (Seabird Information Network, 2015) as described and evaluated in Wentworth et al. (2016) and Croft et al. (submitted). Our simulations include secondary organic aerosol (SOA), both biogenic (~19 Tg yr^{-1}) and enhanced anthropogenic non-volatile (100 Tg yr^{-1}) spatially correlated with anthropogenic CO emissions (D'Andrea et al., 2013).

The TOMAS microphysics scheme tracks the number and mass of particles within each of 15 dry size sections. The first 13 size sections are logarithmically spaced, including aerosol dry diameters from approximately 3 nm to 1 μm, while 2 additional size sections represent aerosol dry diameters from 1 μm to 10 μm (Lee and Adams, 2012). Simulated aerosol species are sulphate, sea-spray, hydrophilic organics, hydrophobic organics, internally mixed black carbon, externally mixed black carbon, dust and water. Aerosol hygroscopic growth is a function of grid box mean relative humidity (RH) capped at 99%. Simulated aerosols are treated as dry (RH=0%) for comparison with the measurements presented in this study

For these simulations, NPF is treated according to the state-of-the-science ternary H_2SO_4-NH_3-H_2O nucleation scheme described by Baranizadeh et al. (2016). The formation rate of particles at circa 1.2 nm in mass diameter is determined from a full kinetics simulation

by Atmospheric Cluster Dynamics Code (ACDC; Olenius et al., 2013) using particle evaporation rates based on quantum chemistry. The scheme is implemented as a comprehensive look-up table of simulated formation rates as a function of sulphuric acid and ammonia vapour concentrations, relative humidity, temperature, and condensation sink for condensable vapours (existing aerosol surface area). Growth and loss of particles with diameters smaller than 3 nm are approximated with the Kerminen et al. (2004) scheme (evaluated in TOMAS in Lee et al. (2013a)). In our simulations, we do not include NPF by organic vapours such as those arising from the oceans (O'Dowd and de Leeuw, 2007; Fu et al., 2013). Currently, no single nucleation scheme includes contributions from organics, sulphuric acid, bases, and water. As well, Giamarelou et al. (2016) found that nucleation-mode particles in the Arctic are predominantly ammonium sulphates.

Growth of simulated particles occurs by condensation of sulphuric acid and organic vapours, which we assume to be non-volatile. These vapours condense proportional to the Fuchs-corrected aerosol surface area distribution (Donahue et al., 2011, Pierce et al., 2011, Riipinen et al., 2011). Condensational growth is not a sink for aerosol number but does transfer aerosol number between size bins while increasing aerosol mass. Coagulation is an important sink for aerosol number (particularly for aerosols with diameters smaller than 100 nm), and moves aerosol mass to larger sizes. Our simulations use the Brownian coagulation scheme of Fuchs (1964), and consider coagulation between all particle sizes.

In our simulations, aerosols are removed from the atmosphere by precipitation both in and below clouds (Liu et al, 2001), and also by dry deposition using a resistance in-series approach (Wesley, 1989) assuming an aerosol dry deposition velocity of 0.03 cm s^{-1} over snow and ice. Wet deposition is an important sink process for aerosols larger than about 50-100 nm in diameter. The in-cloud wet scavenging parameterization in the standard GEOS-Chem-TOMAS module uses the same equations for the removal efficiency and the precipitation fraction as in the bulk-aerosol GEOS-Chem module described in Liu et al. (2001) with updates implemented by Wang et al., (2011) to account for wet removal in mixed-phase and ice clouds. The aerosol in-cloud wet removal in GEOS-Chem-TOMAS is limited to the aerosol size range that is assumed activated into cloud hydrometeors.

2.4 Simulations and revisions to model parameterizations

Table 1 summarizes the four simulations conducted with the GEOS-Chem-TOMAS model. These simulations include 1) a standard, 2) updates to wet removal, 3) updates that add the process of interstitial coagulation of aerosols in clouds, and 4) a sensitivity test with no NPF. The first (simulation STD) uses the standard GEOS-Chem-TOMAS model as described above.

Simulation NEWSCAV introduces developments to the wet removal parameterization to allow for variable in-cloud water content, to implement a temperature-dependent aerosol activation fraction, and to more closely relate in-cloud aerosol scavenging to cloud fraction. The standard GEOS-Chem-TOMAS wet removal efficiency β for large-scale

clouds is based on a parameterization originally developed by Giorgi and Chameides (1986):

$$\beta = k_{min} + Q/L \quad \text{Eq. 1}$$

where Q is the grid- box mean precipitation production rate [g cm^{-3} s^{-1}] from the GEOS-5 meteorological fields, L is the in-cloud liquid and ice water content [g cm^{-3}] of the precipitating clouds (an assumed constant) and *kmin* is a constant, $1x10^{-4}$ s^{-1}. The k_{min} term represents autoconversion processes that produce precipitation. The Q/L term represents accretion processes. The standard GEOS-Chem model uses a globally fixed value for L of $1x10^{-6}$ g cm^{-3}. While this value performs well for wet scavenging in a global sense (Liu et al., 2001; Wang et al., 2011), the value does not well represent observations in certain regions. Measurements by Shupe et al. (2001) and Leaitch et al. (2016) show an Arctic spring-summer-mean cloud liquid water content that is an order of magnitude lower ($1x10^{-7}$ g cm^{-3}). During the spring and summer, more efficient aerosol removal in liquid clouds plays a key role in the control of aerosol distributions (Garrett et al., 2010). An overestimation of the liquid water content of Arctic clouds (by using a globally fixed value for L) in our simulation would yield under-vigorous wet removal efficiency, particularly for cases of low intensity precipitation (low Q). To address this issue, we replace the fixed value with the cloud liquid and ice water contents from the GEOS-5 assimilated meteorology fields and calculate the efficiency as the ratio of the grid-mean precipitation production rate and the grid-mean liquid and ice water contents. We impose a maximum efficiency ($1x10^{-3}$ s^{-1}) to prevent over-vigorous

285 removal. This value is consistent with the upper limit for these process rates given in
286 Gettelman et al. (2013).
287
288 In addition, we implement a temperature-dependent representation of the aerosol
289 activated fraction (Verheggen et al., 2007) to account for the fraction of aerosol
290 susceptible to wet removal in mixed-phase clouds. In mixed-phase clouds, only a fraction
291 of the aerosols are contained in the cloud hydrometeors and susceptible to removal when
292 cloud water and ice converts to precipitation. As clouds glaciate, cloud droplets evaporate
293 and release aerosols from the condensed phase because ice crystals grow at the expense
294 of cloud droplets due to differences in the saturation vapour pressure over liquid water
295 and ice. The Verheggen et al. (2007) parameterization for activated fraction accounts for
296 this effect, such that only a fraction of the total in-cloud aerosol is susceptible to wet
297 removal as precipitation forms in mixed phase clouds. However, in strongly riming-
298 dominated regimes, this may lead to an under-estimate of the removal.
299
300 We also develop the representation of the precipitation fraction. In the standard GEOS-
301 Chem model, the fraction of the grid box that is precipitating, F, is
302
303 $F = Q/\beta L$ Eq. 2
304
305 Replacing β with Eq. 1 and simplifying yields
306
307 $F = 1/(1+(k_{min}L/Q))$ Eq. 3
308

309 where $k_{min}L$ has a fixed value of $1x10^{-10}$ g cm^{-3} s^{-1} in the standard model version. Thus,
310 the precipitation fraction increases with precipitation production rate. We replace this
311 parameterization by treating the precipitation fraction for aerosol scavenging in clouds as
312 the cloud fraction from the GEOS-5 meteorological fields in the model layers where
313 precipitation is produced. These wet scavenging developments were also implemented in
314 a GEOS-Chem v9-03-01 simulation of ^{137}Cs (also using GEOS5 met fields) and
315 evaluated against ^{137}Cs measurements taken for several weeks following the March 2011
316 Fukushima Dai-Ichi nuclear power plant accident. Implementation of these scavenging
317 revisions yielded improved agreement with the radionuclide measurements (median ratio
318 of measured to modeled surface layer concentrations changed from 5.53 to 0.52) and
319 reduced e-folding times from 21.8 days to 13.2 days, which is close to the measurement
320 value of 14.3 days (Kristiansen et al., 2015). These wet removal revisions also slightly
321 reduced the mean bias relative to measurements of the number of aerosols larger than 40
322 nm (N40), 80 nm (N80) and 150 nm (N150) for the same global set of 21 geographically
323 diverse sites as described in D'Andrea et al. (2013) (not shown).
324
325 Simulation NEWSCAV+COAG includes additional developments to the interstitial
326 aerosol coagulation mechanism in clouds for the TOMAS microphysics scheme as
327 explored in Pierce et al. (2015). This revised coagulation parameterization accounts for
328 the order 100-fold increase in the wet size of aerosols that activate to form cloud
329 droplets. This simulation assumes for the purposes of coagulation only that 1) aerosols
330 that activate to form cloud droplets must have a dry diameter larger than 80 nm, 2) super-
331 cooled clouds persist to temperatures as low as 238K and 3) all cloud droplets are 10 μm
332 in diameter. While these are crude assumptions, they are within reasonable bounds and

allow examination of the potential of interstitial coagulation to control aerosol size distributions. The grid-box mean coagulation kernel between two size bins is calculated as

$$J_{i,j} = (1-f_{cloudy})K_{clear;i,j,}N_iN_j + f_{cloudy}K_{cloudy;i,j}N_iN_j \quad \text{Eq. 4}$$

where $J_{i,j}$ is the coagulation rate between particles in bins i and j, f_{cloudy} is the fraction of the grid box that is cloudy, K_{clear} is the coagulation kernel between bins i and j in the clear portion of the gridbox, K_{cloudy} is the coagulation kernel between bins i and j in the cloudy portion of the gridbox, N_i is the number concentration of particles in bin i, and N_j is the number concentration of particles in bin j. While the activated particle is treated as having a diameter of 10 μm, the unactivated collision-partner aerosol is treated as having a diameter following hygroscopic growth under grid-box mean relative humidity. If the in-cloud relative humidity is considerably greater than the grid mean, then the coagulation kernel could be overestimated. These developments to the interstitial aerosol coagulation parameterization in clouds are applied and evaluated in Pierce et al. (2015) and yielded improved agreement with in-situ aerosol size distributions at 21 geographically diverse sites in the Northern Hemisphere.

Simulation NONUC turns off new particle formation (NPF) globally to examine the contribution of NPF to aerosol number in the Arctic. This simulation is otherwise identical to simulation NEWSCAV.

3. Observations and GEOS-Chem-TOMAS simulations of annual cycles in Arctic aerosol number and size

3.1 Observed annual cycle in Arctic aerosol number and size

Figure 1 shows the 2011-2013 monthly median aerosol number distributions from the SMPS at Alert and DMPS at Mt. Zeppelin. At both sites, the accumulation mode (defined here as particles with diameters from 0.1 μm to 0.5 μm due to instrument range, although typically extending to 1 μm) gradually builds during winter to a maximum in March and April. Afterward, the accumulation mode decreases while the Aitken mode (defined here as particles of 0.02 μm to 0.1 μm in diameter due to instrument range, although typically extending to 0.01 μm) increases in number to a maximum in July-August. October is characterized by the lowest number concentrations in both modes until the accumulation mode starts to build again in November. As a result, the total aerosol number at both locations has a shallow maximum in both spring and summer. In Fig. 1, the magnitude between the 20th to 80th percentiles for particles smaller than 100 nm is greatest during the months of June to August when NPF processes in the Arctic boundary layer are expected to make strong and episodic contributions to the aerosol number (e.g. Korhonen et al., 2008; Leaitch et al., 2013). The complete annual cycle is remarkably similar at both sites and similar to that observed at Mt. Zeppelin over an earlier ten-year period from 2000 to 2010 (Fig. 7 in Tunved et al., 2013). The similarity in these number distributions across the one thousand km that separates Alert and Mt. Zeppelin suggests an annual cycle that spans the high Arctic. In the following sections we use the GEOS-Chem-TOMAS model to interpret the processes that control these cycles.

Figure 2 shows the monthly median aerosol effective diameter calculated from the 2011-2013 measurements with SMPS at Alert, and DMPS at Mt. Zeppelin. The effective diameter is the ratio of the second and third moments of the aerosol number distribution, and is useful in determining the optical properties of an aerosol distribution, and for comparing between distributions. The effective diameter is defined as

$$D_{eff} = \int_{Dmin}^{Dmax} D^3 N(D) dD \;\; / \;\; \int_{Dmin}^{Dmax} D^2 N(D) dD \qquad \text{Eq. 5}$$

where D is the aerosol diameter and $N(D)$ is the aerosol number distribution. The integral here is taken over the instrument size range from D_{min} = 20 nm to D_{max} = 500 nm. Despite the geographic distance of these two sites, the annual cycle of the aerosol effective diameter is remarkably similar. At both sites, the aerosol effective diameter shows a strong annual cycle with a minimum during the summer months of about 180 nm and a maximum in the winter of about 260 nm. The effective diameter at Mt. Zeppelin exceeds Alert by about 10-20% throughout the year. In the next sections, we interpret these observed annual cycles in number and size using the GEOS-Chem-TOMAS model.

3.2. Interpreting processes controlling the annual cycle of aerosol number and size with GEOS-Chem-TOMAS

Figures 3 and 4 show the seasonal-median number distributions from measurements at Alert and Mt. Zeppelin, respectively, for winter (DJF), spring (MAM), summer (JJA), and fall (SON), and also for our four simulations. The measurement distributions exhibit

the key features of Arctic aerosol size distributions, a dominant Aitken mode in summer, a dominant accumulation mode with suppressed Aitken mode in non-summer seasons, and minimum number in fall. To assist in interpreting Figs. 3 and 4, we calculate the fractional bias between the observed and simulated total number of aerosols over two size ranges available from the measurement data: 1) Aitken particles 20-100 nm in diameter and 2) accumulation particles 100-500 nm in diameter. We apply a size limit of 20-500 nm to the Mt. Zeppelin measurement data and to our simulations to be consistent with the available data from Alert. We define fractional bias (*FB*) as

$$FB = (C_m - C_0)/C_0 \quad \text{Eq. 6}$$

where C_m is the model value and C_0 is the observed value. These seasonal fractional bias values are presented in Tables 2 and 3. Among all four simulations, simulation STD never has the fractional bias closest to zero for the size ranges considered in Tables 2 and 3.

The strong control of wet removal on Arctic aerosol number and size distributions throughout the annual cycle is highlighted by comparison of simulations STD and NEWSCAV in Figs. 3 and 4 and in Tables 2 and 3. For both Alert and Mt. Zeppelin, the standard GEOS-Chem-TOMAS model (simulation STD) overestimates the observed number of 100-500 nm diameter particles in all seasons as quantified by the positive fractional bias values in Tables 2 and 3. At both Alert and Mt. Zeppelin, this bias is reduced in spring and summer for simulation NEWSCAV relative to STD. The bias reduction is greatest in summer when aerosol wet removal by precipitation is more efficient within the Arctic boundary layer, and strongly limits the accumulation-mode

number at the surface sites. The efficiency of wet removal is parameterized to increase with temperature (from 238 K to 273 K) in our simulations. In seasons other than summer, wet removal in the Arctic boundary layer is less efficient. However, wet removal outside the Arctic boundary layer continues to influence the number of accumulation-mode particles transported to the measurement sites. Over a limited size range (200-500 nm diameter particles) and in all seasons at both sites, NEWSCAV is a closer match to measurements than STD, but the difference between STD and NEWSCAV is very small at Alert in winter and spring.

Wet removal also has feedbacks that particularly influence Aitken-mode and 100-200 nm diameter particle numbers indirectly through changes in NPF and subsequent particle growth to these sizes. Figures 3 and 4 show that at both sites and in all seasons, more vigorous wet removal in simulation NEWSCAV relative to STD yields more numerous Aitken-mode particles (although the springtime difference is very small), and in fall and winter, also more numerous 100-200 nm particles. A reduction in surface area of 200-500 nm aerosols by more vigorous wet removal (simulation NEWSCAV relative to STD) promotes NPF and particle growth. Other than in summer, this NPF occurs primarily outside the Arctic boundary layer and growth occurs during transport to the measurement sites. As a result of the increase in number of 20-200 nm particles in simulation NEWSCAV relative to STD, the accumulation-mode bias is greater for NEWSCAV in fall and winter at both sites and the Aitken mode bias is greater for NEWSCAV in fall, winter and spring at both sites (Tables 2 and 3).

448 The balance of these processes of NPF, growth, and wet removal is a challenge for Arctic
449 simulations of number and size. In all seasons at both sites (except for summer at Mt.
450 Zeppelin), NEWSCAV strongly over estimates the number of 20-40 nm diameter
451 particles. Nonetheless, among the four simulations NEWSCAV has the closest-to-zero
452 bias for the 20-100 nm and 100-500 nm diameter particles at Mt. Zeppelin in summer. As
453 well, at Alert, the summertime Aitken-mode bias for simulation NEWSCAV is second
454 smallest (after NEWSCAV+COAG), but the shape of the distribution shown in Fig. 3 is
455 not a perfect match with the observations for either simulation as there are sizes that are
456 strongly over- and under-predicted within the 20-100 nm diameter range.
457
458 Figures 3 and 4 demonstrate the importance of in-cloud coagulation
459 (NEWSCAV+COAG relative to NEWSCAV) in reducing the number of 20-200 nm
460 diameter particles in all seasons but to varying degrees. In spring and summer at both
461 sites, this additional coagulation for simulation NEWSCAV+COAG reduces the number
462 of 40-100 nm diameter particles excessively relative to measurements. As a result,
463 simulation NEWSCAV is a somewhat better match to measurements in this 40-100 nm
464 diameter range in spring and summer at both sites. However among the four simulations,
465 NEWSCAV+COAG has the smallest fractional bias for the Aitken mode in winter and
466 summer at Alert, and in winter and spring at Mt. Zeppelin, as well as the smallest
467 springtime accumulation-mode bias at both sites (and smallest summertime
468 accumulation-mode bias at Alert).
469
470 Simulation NONUC was designed as a means to assess the relative contribution of NPF
471 processes to the Arctic aerosol size distributions. In our simulations, NPF contributes

most strongly to the number of particles smaller than 200 nm. These contributions occur in all seasons as shown by the differences between NEWSVAC and NONUC in Figs. 3 and 4. In the summertime, NPF occurs within the Arctic boundary layer both in our simulations and in observations (Chang et al, 2011; Leaitch et al., 2013; Allan et al., 2015; Croft et al., submitted). At this time of year, the Arctic region has greater production of oxidants such as OH and has greater dimethyl sulphide (DMS) emissions from the oceanic biological activity, such that oxidation of DMS by OH produces sulphur dioxide (SO_2) and ultimately, sulphuric acid, which contributes to particle formation processes in the boundary layer (e.g. Leaitch et al., 2013). In seasons other than summer, transport of particles arising from NPF outside the Arctic or NPF above the Arctic boundary layer contribute more to the number of particles with diameters smaller than 200 nm. The NONUC simulation coincidentally has lowest bias for the accumulation-mode number in fall and winter at both sites, and for the Aitken mode in fall at both sites, as well as in spring at Alert. Shutting off the NPF process (a source term) in the model appears to compensate for errors in the key sink terms for aerosol number, such as wet removal and coagulation, and related feedbacks. In reality, NPF makes a significant contribution to the number concentration in the Arctic (e.g. Chang et al., 2011; Leaitch et al., 2013). The Arctic is a challenging region that tests the performance of the entire set of model mechanisms. Nevertheless, our results, presented in Figs. 3 and 4, highlight NPF and particle growth, wet removal, and coagulation as key processes for controlling Arctic aerosol size distributions throughout the annual cycle.

Figures 5 and 6 show the annual cycle of the monthly median total number of particles with diameters between 20-500 nm (N20), 80-500 nm (N80), and 200-500 nm (N200) from simulations and from measurements at Alert and Mt. Zeppelin. To assist with interpreting Figs. 5 and 6, Tables 4 and 5 contain the mean fractional bias (MFB) and mean fractional error (MFE) following Boylan and Russell (2006).

$$MFB = \frac{1}{N}\sum_{i=1}^{i=N}\frac{(C_m(i) - C_o(i))}{(C_m(i) + C_o(i))/2}$$

Eq. 7

$$MFE = \frac{1}{N}\sum_{i=1}^{i=N}\frac{|C_m(i) - C_o(i)|}{(C_m(i) + C_o(i))/2}$$

Eq. (8)

where $C_m(i)$ is the i^{th} monthly model value, $C_o(i)$ is the i^{th} monthly measurement value and N is the total number of months in a year.

Figures 5 and 6 demonstrate the key features of the annual cycle of integrated Arctic aerosol number distributions. Measurements from both Alert and Mt. Zeppelin show a shallow maximum in the N20 in both spring and summer. The measurement N80 and N200 have a maximum in March-April at both sites. The minimum for the N20, N80 and N200 from measurements occurs near September-October at both sites. All four simulations capture the general trend of N80 and N200 being higher in spring than in fall, but there are some notable mismatches discussed below.

512 Similar to our findings in examining the seasonal-mean size distributions (Figs 3 and 4),
513 Figs. 5 and 6 show that the N200 is highly sensitive to the wet removal parameterization.
514 Simulation STD over-predicts the N200 at both Alert and Zeppelin as evidenced by the
515 greatest magnitude of the N200 MFB and MFE among the four simulations at both sites
516 for simulation STD. Wet removal revisions for simulation NEWSCAV reduce the N200
517 MFB and MFE towards zero, whereas implementation of the new coagulation mechanism
518 has a lesser effect on these N200 biases. NONUC has the closest-to-zero MFB for N200
519 among the four simulations at both Alert and Zeppelin and also the lowest MFE at Alert.
520 However, the MFE for the N200 is similar between NONUC and NEWSCAV+COAG at
521 both sites. As noted earlier, suppressing particle formation in NONUC likely
522 compensates for errors in sink processes.
523
524 The N20 and N80 are sensitive to the wet removal and coagulation schemes. Tables 4 and
525 5 show that interstitial coagulation (NEWSCAV+COAG relative to NEWSCAV) reduces
526 the MFB and MFE, for N20 and N80 at both Alert and Mt. Zeppelin. However, changes
527 to the wet-removal parameterization increase the N20 and N80 MFB and MFE at both
528 sites for simulation NEWSCAV relative to STD, except for the N80 MFB at Mt.
529 Zeppelin. As discussed in reference to Figs. 3 and 4, NPF increases when the wet
530 removal is more vigorous, and these new particles grow to increase the number of
531 Aitken-mode aerosols in the simulations (i.e. the condensation sink for condensable
532 vapours on to existing aerosols is lower, which favours NPF and growth and reduces
533 losses of new particles by coagulation). At Mt. Zeppelin for the N20 and N80, NONUC
534 has the smallest MFB but NEWSCAV+COAG best represents the annual cycle (smallest

535 MFE) among the four simulations. At Alert, for the N20 and N80, NEWSCAV+COAG
536 best represents the annual cycle (smallest MFE and MFB).
537
538 Figures 5 and 6 also show the annual cycle of aerosol effective diameter at both Alert and
539 Mt. Zeppelin for our simulations and from measurements. The simulation
540 NEWSCAV+COAG has the closest agreement (smallest MFE) with the annual cycle of
541 effective diameter from the measurements for both sites. At Alert, the aerosol effective
542 diameter has the smallest bias for both NEWSCAV and NEWSCAV+COAG, whereas, at
543 Mt. Zeppelin, STD has the smallest bias for the effective diameter due to cancellation of
544 errors between months of over- and under-prediction. The simulations over-predict the
545 aerosol effective diameter in July and August, except for NEWSCAV at Mt. Zeppelin.
546 The over-prediction of summertime effective diameter is pronounced for the simulation
547 NONUC that removes NPF, illustrating the importance of NPF in yielding the
548 summertime minimum effective diameter. The effective diameter in winter at Mt.
549 Zeppelin is strongly underestimated in all simulations, reflecting too many small (Aitken
550 mode) particles, even for simulation NONUC.
551
552 The similarity in the annual cycle of effective diameter from measurements at both Alert
553 and Zeppelin suggests a cycle that occurs throughout the Arctic. Figure 7 shows the
554 seasonal-mean pan-Arctic geographic distribution of the surface layer effective diameter
555 for the NEWSCAV+COAG simulation. Throughout the Arctic, the simulated effective
556 diameter declines to a minimum in summer. In Fig. 7, we superimpose the effective
557 diameter from observations at Alert and Mt. Zeppelin. The simulated effective diameter

at the altitude of Mt Zeppelin (500 m) is smaller than the surface value shown here (by 35 nm in summer, 20 nm in fall and 5 nm in winter and spring).

3.3. Process rates controlling the annual cycle in Arctic aerosol number and size

Figure 8 shows the monthly- and regional-mean process rates that control aerosol number in four size ranges for the entire troposphere north of the Arctic Circle (66 °N) for simulation NEWSCAV+COAG. Source processes for aerosol number are positive and sink processes are negative.

The number of aerosols smaller than 10 nm in diameter (nucleation-mode size) is primarily controlled by NPF (particle formation, also termed nucleation), coagulation, and transport. There are two maxima in the particle formation rate shown in Fig. 8 (top-left panel), one in early spring (March) and one in summer (July). In spring, simulated NPF occurs mainly in the free troposphere, whereas in summer, NPF occurs also in the boundary layer. In the summertime Arctic boundary layer, NPF is enhanced by the low aerosol surface area due to efficient wet removal of accumulation-mode aerosols by episodic rain and summer enhancements in sulphuric acid production rates (from oxidation of DMS). The simulated early-spring NPF rate maximum for nucleation-size particles is associated with NPF in the middle and upper troposphere, and as a result is not evident in the measurements at Alert and Mt. Zeppelin. This simulated springtime maximum in NPF occurs because the precursors for sulphuric acid (DMS, SO_2) are

transported from open ocean areas and pollution sources at lower latitudes. Then NPF proceeds in locations where the condensation sink for sulphuric acid on existing aerosols is low such as following wet scavenging episodes.

The top-left panel of Fig. 8 shows that transport reaches a maximum during winter, while NPF reaches a minimum such that the two are comparable sources for the entire Arctic troposphere. Simulated NPF occurs in the dark Arctic wintertime since the oxidant OH is produced through reaction of ozone and volatile organic compounds, although the OH mixing ratios are three-fold less than in summer. As a result, sulphuric acid (a particle precursor vapour) can be produced though oxidation by OH of DMS and sulphur dioxide (SO_2) transported into the Arctic in winter. Our simulated Arctic wintertime sulphuric acid mixing ratio is about 0.01 ppt near the tropopause and diminishes towards the Earth's surface. Measurements by Möhler and Arnold (1992) indicate wintertime sulphuric acid levels in Northern Scandinavia of about 0.1 ppt near the tropopause decreasing to 0.01 ppt near the Earth's surface, implying the true nucleation rate could be even higher.

Figure 9 shows aerosol number transport rates at different altitudes by decomposing the rates from Fig. 8 into four altitude bands. Nucleation-mode particles are mostly transported in the mid to upper troposphere (at altitudes between 4 and 10 km) where the coagulation sink is sufficiently low that nucleation-mode particles can persist. At these altitudes and particularly when the atmosphere just been cleaned by a precipitation event, if the Aitken- and accumulation-mode concentrations are low (5-10 cm^{-3}), then nucleation-mode particles can have a lifetime of about one week with respect to loss by

coagulation. Transport rates for nucleation size-particles are greatest from January to March.

Figure 8 (top-right panel) indicates that several processes control the simulated Aitken-mode number in the Arctic troposphere. Northward transport is the dominant source process for the Arctic Aitken mode during all months of the year. This transport of simulated Aitken-mode aerosols occurs throughout the troposphere as shown in Fig. 9. Figure 8 shows that during the Arctic spring (March-April), when the total aerosol mass is greatest, condensational growth of existing aerosols makes a relatively greater contribution to the total source rates for Aitken-mode particles. This net enhancement in condensational growth includes condensational loss of Aitken-mode particles to accumulation-mode sizes such that the nucleation mode is a larger source of Aitken-mode particles than apparent in the figure. Simulated primary particle emissions within the Arctic have a relatively constant source rate for the Aitken mode throughout the year, quite similar in magnitude to the maximum condensational growth rate in March-April. Coagulation is the dominant sink for the Aitken mode with dry deposition accounting for the majority of the remaining sink. Simulated removal of the Aitken- mode number by wet deposition is a weaker sink than dry deposition because the smaller Aitken-mode aerosols have inefficient removal by activation scavenging (the process of aerosols acting as the seed for cloud-droplet and ice-crystal formation and subsequent removal during precipitation). Recent studies indicate that aerosols as small as 50 nm - 60 nm can activate in the clean Arctic summertime conditions (Leaitch et al., 2013; Leaitch et al., 2016) and we likely under-estimate this removal in our simulations. Figure 8 does show an increase in wet removal as a sink for the Aitken mode in summer as this process

becomes more efficient at warmer temperatures and aerosols larger than about 60 nm are removed by activation scavenging in our simulations.

For the accumulation-mode particle number simulation, Fig. 8 (bottom-left panel) indicates that the dominant sources are northward transport and condensational growth, which also includes production of sulphate by in-cloud oxidation. These two simulated source terms are roughly equal in magnitude in the Arctic throughout April to October. Northward transport of accumulation-mode aerosols persists in the simulation in all seasons, with a minimum in winter and an increase in March-April. Figure 9 shows that transport of accumulation size aerosol at altitudes between 1.5 km and 4 km reaches a maximum in April, which would contribute to the well-known Arctic haze phenomena. Figure 9 also shows that the majority of simulated accumulation-mode number transport is below 1.5 km. This low-level transport is persistent though diminished throughout the summer; suggesting that the summertime cleanliness of the Arctic near-surface atmosphere relies heavily on the increased efficiency of the removal processes in the lower troposphere during the summer months. Indeed, Fig. 8 shows that wet removal is the dominant accumulation aerosol number sink process in all seasons, but increases in magnitude and relative importance with respect to dry deposition in the summer, accounting for about 90% of the total summertime sink rate. In winter, the relative simulated importance of dry deposition for accumulation aerosol number increases, although remains below 25% of the total sink rate.

Since wet removal has large effects on the accumulation aerosol number associated with Arctic springtime pollution, we further examined its annual cycle. Figure 10 shows the

653 monthly- and regional-mean accumulation-mode number lifetime with respect to wet
654 removal for layers of the lower troposphere. Longer lifetimes from December to March
655 contribute to the build up of the Arctic haze layer, particularly as this is combined with
656 transport of pollution into the Arctic during wintertime. The spring to summer transition
657 period is characterized by a rapid increase in the efficiency of wet scavenging that
658 contributes to removal of the Arctic haze in April-May. Figure 10 shows about a 5-fold
659 decrease in wet removal lifetime in the Arctic 1.5-4 km layer from February to April.
660 Simulated wet removal lifetimes in the Arctic boundary layer below 1.5 km reach a
661 minimum in October, such that when combined with diminishing new particle formation
662 as the sunsets and limited transport yields the simulated total aerosol number minimum in
663 the fall season, similar to that observed at Alert and Mt. Zeppelin. To put the Arctic
664 region in context, Fig. 10 also shows the lifetimes with respect to wet removal for the
665 region north of 50°N, indicating that wet removal processes are generally more efficient
666 for a region with greater southward extent and at lower altitudes.
667
668 Figure 8 shows that the simulated coarse mode is controlled primarily by emissions,
669 transport and wet deposition. In early spring (March-April), northward transport of
670 coarse-mode aerosols (dust and sea-salt emissions) is not quite matched by the removal
671 processes. The resultant residual (black line on Fig. 8) gives the net rate of either aerosol
672 build-up or loss for the regional monthly mean number. In early spring, there is a net
673 build-up of coarse-mode aerosol in the Arctic region. However as spring progresses, there
674 is a net loss such that the net residual integrates to zero over the annual cycle. Wet
675 removal is the primary loss process in all seasons in this simulation. Figure 9 shows that

676 the early springtime transport of the coarse mode occurs mainly at altitudes between 1.5
677 and 4 km, a time when the polar dome still extends relatively far southward.
678
679 In this section we examined process rates over the entire troposphere north of 66 °N. To
680 put these Arctic process rates in context with other regions, Fig. 11 shows the same set of
681 processes for the same four aerosol size ranges over the entire troposphere north of
682 50 °N. Several differences are apparent. For the nucleation, Aitken and accumulation
683 sizes, transport is of negligible importance relative to other source processes, unlike for
684 the Arctic region. Coagulation remains the main sink for the number of nucleation- and
685 Aitken-mode aerosols as shown in Figs. 8 and 11, but the relative importance of wet
686 removal of the Aitken mode in summer has diminished. Wet removal rates for the
687 accumulation-mode aerosol number reach a maximum in May in the Arctic whereas the
688 maximum is in July for the entire region north of 50°N. For the Aitken and accumulation
689 modes, condensational growth is the dominant source north of 50 °N, unlike for the
690 Arctic region only (Fig. 8) where transport was of similar or greater importance. The
691 coarse mode north of 50 °N shows a peak in the transport source in April, similar to Fig.
692 8, associated with transport of dust from lower latitudes in spring. Coarse-particle number
693 wet removal also shows an April maximum in both Figs. 8 and 11. The global mean
694 simulated number process rates (not shown) show a relative importance of processes
695 similar to that in Fig.11, except in the global mean, primary emissions are the only non-
696 negligible source of coarse aerosol number throughout the year. Wet deposition remains
697 the dominant sink of accumulation and coarse-mode number, followed by dry deposition
698 at the global scale, as in the Arctic.

4. Conclusions

In this study, we examined the annual cycle of aerosol number and size distributions in the Arctic from measurements made during 2011-2013 by scanning mobility particle sizer (SMPS) at Alert and by differential mobility particle sizer (DMPS) at Mt. Zeppelin. There was a strong and similar annual cycle in measurements of aerosol number and size at both sites despite their geographic separation of 1000 km. The annual cycle in the total number of aerosols larger than 20 nm had two maxima. The maximum in spring was dominated by accumulation-mode aerosols (particles 100 nm to 500 nm in diameter) and in summer was dominated by Aitken-mode aerosols (particles 20 nm to 100 nm in diameter). At both sites, total aerosol number reached a minimum in October. The annual cycle of aerosol effective diameter derived from measurements had an inter-seasonal range between 180 nm and 260 nm, with a minimum in the summer. These annual cycles were similar to those presented by Tunved et al. (2013) based on earlier data at Mt. Zeppelin between the years 2000 and 2010.

We interpreted these annual cycles in Arctic aerosol number and size with the GEOS-Chem-TOMAS aerosol microphysics model. Our simulations indicated a strong sensitivity of the annual cycle of Arctic aerosol number and size to several key processes; new-particle formation (NPF), interstitial coagulation scavenging in clouds, wet removal through precipitation, and transport.

721 Our GEOS-Chem-TOMAS simulations demonstrated that wet removal had a strong
722 control on Arctic aerosol number distributions throughout the annual cycle, similar to the
723 findings of earlier studies focused on spring-summer (Korhonen et al, 2008) and Arctic
724 aerosol mass abundance (e.g. Garrett et al., 2010; Browse et al., 2012; Sharma et al.,
725 2013). In our study, wet removal updates were developed for the GEOS-Chem-TOMAS
726 model that together increased the efficiency of wet removal. We replaced the global-
727 constant cloud liquid water content with the values from GEOS-5 assimilated
728 meteorology fields, updated the gridbox precipitation fraction, and implemented the
729 Verheggen et al. (2007) temperature-dependent aerosol activation fraction to account for
730 the fraction of aerosol assumed to be susceptible to wet removal in mixed-phase clouds.
731 In our updated-removal simulation, efficient wet removal in the Arctic summertime
732 boundary layer strongly limited the accumulation-mode number despite an ongoing
733 source through transport and condensational growth. The wet removal updates reduced
734 model-measurement bias (relative to the standard model) for the number of aerosols
735 larger than 200 nm in all seasons at both Alert and Mt. Zeppelin (although the changes in
736 winter and spring at Alert were relatively small).
737
738 More vigorous wet removal promoted NPF and growth in our simulations and
739 contributed to a summertime dominant Aitken mode since a reduction in the surface area
740 of accumulation size aerosols (the condensation sink for sulphuric acid) influences the
741 likelihood that sulphuric acid will participate in NPF as opposed to condensing on
742 existing aerosols. Indeed, the more vigorous wet removal scheme increased the simulated
743 Aitken-mode number in all seasons at Alert and Mt. Zeppelin (although the springtime

744 Aitken mode was relatively less sensitive to the changes made in our study). Outside of
745 summer, NPF and growth occurred mostly outside the Arctic boundary layer. A
746 sensitivity study with no NPF globally indicated that NPF strongly controls the number
747 of particles with diameters smaller than 200 nm in all seasons in the Arctic, while
748 particularly important in yielding the summertime Aitken-mode dominance.
749
750 From February to April, the simulated accumulation-mode wet removal efficiency at
751 altitudes of the springtime Arctic haze layer (between 1.5 and 4 km) increased by 5-fold,
752 contributing to our simulation of the spring-summer transition from Aitken- to
753 accumulated-mode dominated Arctic size distributions (e.g. Engvall et al., 2008;
754 Korhonen et al., 2008). In the boundary layer, simulated wet removal efficiency reached a
755 maximum (lowest accumulation-mode aerosol number lifetime) in October. The observed
756 total aerosol number minimum in October was reproduced in our simulations due to
757 efficient wet removal combined with diminished boundary layer NPF due to lower
758 sulphuric acid concentrations and limited transport.
759
760 We also found an important role for coagulation of interstitial aerosols in clouds with
761 aerosols of larger size that have activated to form cloud droplets. There has been
762 relatively less attention given to the importance of this process in controlling Arctic size
763 distributions despite the Arctic being a region with widespread cloud cover in all seasons.
764 Implementation of an interstitial coagulation mechanism in clouds in our simulations
765 reduced the number of aerosols with diameters smaller than 200 nm in all seasons at both
766 Alert and Mt. Zeppelin. In some seasons this reduction in the Aitken-mode number
767 worsened model-measurement agreement, highlighting the delicate balance between the

768 processes of coagulation, NPF, growth and wet removal in control of the Arctic size
769 distributions that is challenging to simulate. Our simulations tended to under predict the
770 number of larger Aitken-mode aerosols (40-100 nm in diameter) in summer and this is
771 the subject of ongoing investigation related to aerosol sources and growth.
772
773 The high sensitivity of aerosol number to interstitial coagulation in clouds suggests that
774 size-resolved models should include this process. However, many present-day global
775 models neglect this process, including previous versions of GEOS-Chem-TOMAS
776 (D'Andrea et al., 2013; Pierce et al., 2013; Trivitayanurak et al., 2008), GISS-TOMAS
777 (Adams and Seinfeld, 2002; Pierce and Adams, 2009), GLOMAP (Spracklen et al.,
778 2005a,b; 2008, Mann et al., 2012), GLOMAP-Mode (Mann et al., 2010; 2012, Lee et al.,
779 2013b), GEOS-Chem-APM (Yu and Luo, 2009; Yu, 2011) and IMPACT (Herzog et al.,
780 2004; Wang and Penner, 2009). To our knowledge, only a few models such as MIRAGE
781 and ECHAM-HAM (Herzog et al., 2004; Ghan et al., 2006; Hoose et al., 2008) represent
782 this process.
783
784 Our results highlight the importance of aerosol processes (as well as their delicate balance
785 and interactions) that continue to be poorly understood; 1) new-particle formation (NPF)
786 and growth, 2) in-cloud interstitial coagulation, and 3) wet removal as playing a key role
787 in the control of the annual cycle of aerosol number and size in the Arctic. The relative
788 importance of the processes that control aerosol number could change in a future
789 warming Arctic climate and also as emissions within the Arctic change.
790
791

Acknowledgements:

The authors acknowledge the financial support provided for NETCARE through the Climate Change and Atmospheric Research Program at NSERC Canada. Thanks to Sangeeta Sharma, Desiree Toom, Andrew Platt and the Alert operators for supporting the Alert observations. We are also grateful to Ilona Riipinen, Jan Julin and Tinya Olenius for helpful discussions and for providing the Atmospheric Cluster Dynamics Code (ACDC), applied in our GEOS-Chem-TOMAS simulations.

References:

Adams, P. J. and Seinfeld, J. H.: Predicting global aerosol size distributions in general circulation models, J. Geophys. Res., 107(D19), 4310–4370, 2002.

Adams, P. J. and Seinfeld, J. H.: Disproportionate impact of particulate emissions on global cloud condensation nuclei concentrations, Geophys. Res. Lett., 30(5), 1210–1239, 2003.

Albrecht, B. A.: Aerosols, Cloud Microphysics, and Fractional Cloudiness, Science, 245(4923), 1227–1230, 1989.

Baranizadeh, E., Murphy, B. N., Julin, J., Falahat, S., Reddington, C. L., Arola, A., Mikkonen, S., Fountoukis, C., Patoulias, D., Minikin, A., Hamburger, T., Laaksonen, A., Pandis, S. N., Vehkamäki, H., Lehtinen, K. E. J. and Riipinen, I.: Implementation of state-of-the-art ternary new particle formation scheme to the regional chemical transport

817 model PMCAMx-UF in Europe, Geosci. Model, Dev. Discuss., doi:10.5194/gmd-2016-
818 21, 2016.
819
820 Bey, I., Jacob, D. J., Yantosca, R. M., Logan, J. A., Field, B. D., Fiore, A. M., Li, Q., Liu,
821 H. Y., Mickley, L. J. and Schultz, M. G.: Global modeling of tropospheric chemistry with
822 assimilated meteorology: Model description and evaluation, J. Geophys. Res., 106(D19),
823 23073, doi:10.1029/2001JD000807, 2001.
824
825 Boylan, J. W. and Russell, A. G.: PM and light extinction model performance metrics,
826 goals, and criteria for three-dimensional air quality models, Atmos. Environ., 40, 4946-
827 4959, 2006.
828
829 Breider, T. J., Mickley, L. J., Jacob, D. J., Ge, C., Wang, J., Payer, M., Wang, Q., Fisher,
830 J., Ridley, D., McConnell, J., Sharma, S., et al.: 1980-2010 changes in Arctic Radiative
831 Forcing from Aerosols (in prep).
832
833 Browse, J., Carslaw, K. S., Arnold, S. R., Pringle, K. and Boucher, O.: The scavenging
834 processes controlling the seasonal cycle in Arctic sulphate and black carbon aerosol,
835 Atmos. Chem. Phys., 12(15), 6775–6798, doi:10.5194/acp-12-6775-2012, 2012.
836
837 Browse, J., Carslaw, K. S., Mann, G. W., Birch, C. E., Arnold, S. R. and Leck, C.: The
838 complex response of Arctic aerosol to sea-ice retreat, Atmos. Chem. Phys., 14(14), 7543–
839 7557, doi:10.5194/acp-14-7543-2014, 2014.
840

841 Cesana, G., Kay, J. E., Chepfer, H., English, J. M. and de Boer, G.: Ubiquitous low-level
842 liquid-containing Arctic clouds: New observations and climate model constraints from
843 CALIPSO-GOCCP, Geophys. Res. Lett., 39(20), n/a–n/a, doi:10.1029/2012GL053385,
844 2012.
845
846 Chang, R. Y.-W., Leck, C., Graus, M., Müller, M., Paatero, J., Burkhart, J. F., Stohl, A.,
847 Orr, L. H., Hayden, K., Li, S.-M., Hansel, A., Tjernström, M., Leaitch, W. R. and Abbatt,
848 J. P. D.: Aerosol composition and sources in the central Arctic Ocean during ASCOS,
849 Atmos. Chem. Phys., 11, 10619-10636, doi:10.5194/acp-11-10619-2011, 2011.
850
851 Charlson, R. J., Schwartz, S. E., Hales, J. M., Cess, R. D., Coakley, J. A., Hansen, J. E.
852 and Hofman, D. J.: Climate Forcing by Anthropogenic Aerosols, Science., 255(5043),
853 423–430, 1992.
854
855 Croft, B., Wentworth, G., Leaitch, W. R., Kodros, J., Murphy, J. G., Abbatt, J. P. D.,
856 Martin, R. V., and Pierce, J. R.: Contribution of Arctic seabird ammonia to atmospheric
857 particles and cloud radiative effect, Nature Geosci. (submitted).
858
859 D'Andrea, S. D., Hakkinen, S. A. K., Westervelt, D. M., Kuang, C., Levin, E. J. T.,
860 Kanawade, V. P., Leaitch, W. R., Spracklen, D. V., Riipinen, I., and Pierce, J. R.:
861 Understanding global secondary organic aerosol amount and size-resolved
862 condensational behavior, Atmos. Chem. Phys., 13, 11519-11534, doi:10.5194/acp-13-
863 11519-11534, 2013.
864

865 Di Pierro, M., Jaeglé, L., Eloranta, E. W. and Sharma, S.: Spatial and seasonal
866 distribution of Arctic aerosols observed by the CALIOP satellite instrument (2006–2012),
867 Atmos. Chem. Phys., 13(14), 7075–7095, doi:10.5194/acp-13-7075-2013, 2013.
868
869 Donahue, N. M., Trump, E. R., Pierce, J. R., and Riipinen, I.: Theoretical constraints on
870 pure vapour-pressure driven condensation of organics to ultrafine particles, Geophys.
871 Res. Lett., 38, L16801, doi:10.1029/2011GL048115, 2011.
872
873 Engvall, A. C., Krejci, R., Ström, J., Minikin, A., Treffeisen, R., Stohl, A. and Herber, A.:
874 In-situ airborne observations of the microphysical properties of the Arctic tropospheric
875 aerosol during late spring and summer, Tellus, Ser. B Chem. Phys. Meteorol., 60 B(3),
876 392–404, doi:10.1111/j.1600-0889.2008.00348.x, 2008.
877
878 Fu, P. Q., Kawamura, K., Chen, J., Charrière, B. and Sempéré, R.: Organic molecular
879 composition of marine aerosols over the Arctic Ocean in summer: Contributions of
880 primary emission and secondary aerosol formation, Biogeosciences, 10(2), 653–667,
881 doi:10.5194/bg-10-653-2013, 2013.
882
883 Fuchs, N. A.: Mechanics of Aerosols, Pergamon, New York, 1964.
884
885 Garrett, T. J., Brattström, S., Sharma, S., Worthy, D. E. J. and Novelli, P.: The role of
886 scavenging in the seasonal transport of black carbon and sulfate to the Arctic, Geophys.
887 Res. Lett., 38(16), doi:10.1029/2011GL048221, 2011.
888

889 Garrett, T. J., Zhao, C. and Novelli, P. C.: Assessing the relative contributions of
890 transport efficiency and scavenging to seasonal variability in Arctic aerosol, Tellus B,
891 62(3), 190–196, doi:10.1111/j.1600-0889.2010.00453.x, 2010.
892
893 Gettelman, A., Morrison, H., Terai, C. R. and Wood, R.: Microphysical process rates and
894 global aerosol-cloud interaction, Atmos. Chem. Phys., 13, 9855-9867, 2013.
895
896 Ghan, S. J., Rissman, T. A., Elleman, R., Ferrare, R. A., Turner, D., Flynn, C., Wang, J.,
897 Ogren, J., Hudson, J., Jonsson, H. H., VanReken, T., Flagan, R. C. and Seinfeld, J. H.:
898 Use of in situ cloud condensation nuclei, extinction, and aerosol size distribution
899 measurements to test a method for retrieving cloud condensation nuclei profiles from
900 surface measurements, J. Geophys. Res., 111(D5), 2006.
901
902 Giamarelou, M., Eleftheriadis, K., Nyeki, S., Tunved, P., Torseth, K. and Biskos, G.:
903 Indirect evidence of the composition of nucleation mode atmospheric particles in the high
904 Arctic, J. Geophys. Res., 121, doi:10.1002/2015JD023646, 2016.
905
906 Giorgi, F. and Chameides, W. L.: Rainout Lifetimes of Highly Soluble Aerosols and
907 Gases as Inferred From Simulations With a General Circulation Model, J. Geophys. Res.,
908 91(D13), 14367–14376, 1986.
909
910 Haywood, J. M. and Boucher, O.: Estimates of the Direct and Indirect Radiative Forcing
911 Due to Tropospheric Aerosols: A review, Rev. Geophys., (38), 513–543, 2000.
912

913 Heintzenberg, J., Leck, C. and Tunved, P.: Potential source regions and processes of
914 aerosol in the summer Arctic, Atmos. Chem. Phys., 15(11), 6487–6502, doi:10.5194/acp-
915 15-6487-2015, 2015.
916
917 Herzog, M., Weisenstein, D. K. and Penner, J. E.: A dynamic aerosol module for global
918 chemical transport models: Model description, J. Geophys. Res. Atmos., 109,
919 doi:10.1029/2003JD004405, 2004.
920
921 Hoose, C., Lohmann, U., Bennartz, R., Croft, B. and Lesins, G.: Global simulations of
922 aerosol processing in clouds, Atmos. Chem. Phys. Discuss., 8(4), 13555–13618, 2008.
923
924 Kerminen, V. M., Anttila, T., Lehtinen, K. E. J. and Kulmala, M.: Parameterization for
925 atmospheric new-particle formation: Application to a system involving sulfuric acid and
926 condensable water-soluble organic vapors, Aerosol Sci. Technol., 38(10), 1001–1008,
927 2004.
928
929 Korhonen, H., Carslaw, K. S., Spracklen, D. V., Ridley, D. A. and Ström, J.: A global
930 model study of processes controlling aerosol size distributions in the Arctic spring and
931 summer, J. Geophys. Res., 113(D8), 1–20, doi:10.1029/2007JD009114, 2008.
932
933 Kristiansen, N. I., Stohl, A., Olivié, D. J. L., Croft, B., Søvde, O. A. and Klein, H.:
934 Evaluation of observed and modelled aerosol lifetimes using radioactive tracers of
935 opportunity and an ensemble of 19 global models, 24513–24585, doi:10.5194/acpd-15-
936 24513-2015, 2015.

Leaitch, W. R., Korolev, A., Aliabadi, A., Burkhart, J., Willis, M., Abbatt, J. P. D., Bozem, H., Hoor, P., Köllner, F., Schneider, J., Herber, A., Konrad, J., Brauner, R.: Effects of 20-100 nanometre particle on liquid cloud in the clean summertime Arctic, Atmos. Chem. Phys. Discuss. doi:10.5194/acp-2015-999, 2016.

Leaitch, W. R., Sharma, S., Huang, L., Toom-Sauntry, D., Chivulescu, A., Macdonald, A. M., von Salzen, K., Pierce, J. R., Bertram, A. K., Schroder, J. C., Shantz, N. C., Chang, R. Y. W. and Norman, A.-L.: Dimethyl sulfide control of the clean summertime Arctic aerosol and cloud, Elem. Sci. Anth., 1, 17, doi:10.12952/journal.elementa.000017, 2013.

Lee, Y. H. and Adams, P. J.: A Fast and Efficient Version of the TwO-Moment Aerosol Sectional (TOMAS) Global Aerosol Microphysics Model, Aerosol Sci. Technol., 46(6), 678–689, doi:10.1080/02786826.2011.643259, 2012.

Lee, Y.H., Pierce, J.R., Adams, P.J.: Representation of nucleation mode microphysics in global aerosol microphysics models, Geosci. Model Dev., 6, 1221-1232, doi:10.5194/gmd-6-1221-2013, 2013a.

Lee, L. A., Pringle, K. J., Reddington, C. L., Mann, G. W., Stier, P., Spracklen, D. V., Pierce, J. R. and Carslaw, K. S.: The magnitude and causes of uncertainty in global model simulations of cloud condensation nuclei, Atmos. Chem. Phys., 13(17), 8879–8914, doi:10.5194/acpd-13-6295-2013, 2013b.

961 Liu, H., Jacob, D. J., Bey, I. and Yantosca, R. M.: Constraints from 210Pb and 7Be on
962 wet deposition and transport in a global three-dimensional chemical tracer model driven
963 by assimilated meteorological fields, J. Geophys. Res., 106(Dll), 12109–12128, 2001.
964
965 Lohmann, U. and Feichter, J.: Global indirect aerosol effects: a review, Atmos. Chem.
966 Phys. Discuss., 4, 7561–7614, doi:10.5194/acpd-4-7561-2004, 2004.
967
968 Mann, G. W., Carslaw, K. S., Spracklen, D. V., Ridley, D. A., Manktelow, P. T.,
969 Chipperfield, M. P., Pickering, S. J. and Johnson, C. E.: Description and evaluation of
970 GLOMAP-mode: a modal global aerosol microphysics model for the UKCA
971 composition-climate model, Geosci. Model Dev. Discuss., 3, 651–734,
972 doi:10.5194/gmdd-3-651-2010, 2010.
973

974 Mann, G. W., Carslaw, K. S., Ridley, D. A., Spracklen, D. V., Pringle, K. J., Merikanto,
975 J., Korhonen, H., Schwarz, J. P., Lee, L. A., Manktelow, P. T., Woodhouse, M. T.,
976 Schmidt, A., Breider, T. J., Emmerson, K. M., Reddington, C. L., Chipperfield, M. P. and
977 Pickering, S. J.: Intercomparison of modal and sectional aerosol microphysics
978 representations within the same 3-D global chemical transport model, Atmos. Chem.
979 Phys., 12, 4449–4476, doi:10.5194/acp-12-4449-2012, 2012.
980
981 Möhler, O. and Arnold, F.: Gaseous sulfuric acid and sulfur dioxide measurements in the
982 Arctic troposphere and lower stratosphere: Implications for hydroxyl radical abundances,
983 Geophys. Res. Lett., 19, 1763-1766, 1992.
984

985 Napari, I., Noppel, M., Vehkamaki, H. and Kulmala, M.: Parameterization of ternary
986 nucleation rates for H2SO4-NH3-H2O vapors, J. Geophys. Res., 107(D19), 4310–4381,
987 2002.
988
989 O'Dowd, C. D. and de Leeuw, G.: Marine aerosol production: a review of the current
990 knowledge., Philos. Trans. A. Math. Phys. Eng. Sci., 365(1856), 1753–1774,
991 doi:10.1098/rsta.2007.2043, 2007.
992
993 Olenius, T., Kupiainen-Määttä, O., Ortega, I. K., Kurtén, T. and Vehkamäki, H.: Free
994 energy barrier in the growth of sulfuric acid-ammonia and sulfuric acid-dimethylamine
995 clusters, J. Chem. Phys., 139(8), doi:10.1063/1.4819024, 2013.
996
997 Pierce, J.R., Adams, P.J., Uncertainty in global CCN concentrations from uncertain
998 aerosol nucleation and primary emission rates, Atmospheric Chemistry and Physics, 9,
999 1339-1356, 2009.
1000
1001 Pierce, J. R., Riipinen, I., Kulmala, M., Ehn, M., Petäjä, T., Junninen, H., Worsnop, D.
1002 R., and Donahue, N. M.: Quantification of the volatility of secondary organic compounds
1003 in ultrafine particles during nucleation events, Atmos. Chem. Phys., 11, 9019-9036,
1004 doi:10.5194/acp-11-9019-2011, 2011.
1005
1006 Pierce, J.R., Evans, M.J., Scott, C.E., D'Andrea, S.D., Farmer, D.K., Swietlicki, E.,
1007 Spracklen, D.V.: Weak sensitivity of cloud condensation nuclei and the aerosol indirect

1008 effect to Criegee+SO2 chemistry, Atmospheric Chemistry and Physics, 13, 3163-3176,
1009 doi:10.5194/acp-13-3163-2013, 2013.
1010
1011 Pierce, J. R., Croft, B., Kodros, J. K., D'Andrea, S. D. and Martin, R. V.: The importance
1012 of interstitial particle scavenging by cloud droplets in shaping the remote aerosol size
1013 distribution and global aerosol-climate effects, Atmos. Chem. Phys., 15(11), 6147–6158,
1014 doi:10.5194/acp-15-6147-2015, 2015.
1015
1016 Riddick, S. N., Dragosits, U., Blackall, T. D., Daunt, F., Wanless, S. and Sutton, M. a.:
1017 The global distribution of ammonia emissions from seabird colonies, Atmos. Environ.,
1018 55, 319–327, doi:10.1016/j.atmosenv.2012.02.052, 2012.
1019
1020 Riipinen, I., Pierce, J. R., Yli-Juuti, T., Nieminen, T., Häkkinen, S., Ehn, M., Junninen,
1021 H., Lehtipalo, K., Petäjä, T., Slowik, J., Chang, R., Shantz, N. C., Abbatt, J., Leaitch, W.
1022 R., Kerminen, V.-M., Worsnop, D. R., Pandis, S. N., Donahue, N. M. and Kulmala, M.:
1023 Organic condensation: a vital link connecting aerosol formation to cloud condensation
1024 nuclei (CCN) concentrations, Atmos. Chem. Phys., 11, 3865-3878, doi:10.5194/acp-11-
1025 3865-2011, 2011.
1026
1027 Seabird Information Network: Circumpolar Seabird Data Portal, [online] Available from:
1028 http://axiom.seabirds.net/circumpolar_portal.php (Accessed 13 March 2015), 2015.
1029
1030 Sharma, S., Ishizawa, M., Chan, D., Lavoué, D., Andrews, E., Eleftheriadis, K. and
1031 Maksyutov, S.: 16-year simulation of Arctic black carbon: Transport, source contribution,

and sensitivity analysis on deposition, J. Geophys. Res. Atmos., 118(2), 943–964, doi:10.1029/2012JD017774, 2013.

Shindell, D. and Faluvegi, G.: Climate response to regional radiative forcing during the twentieth century, Nature Geosci., 2, 294-300, doi:10.1038/NGEO473, 2009.

Shupe, M. D., Uttal, T., Matrosov, S. Y. and Frisch, A. S.: Cloud Water Contents and Hydrometeor Sizes During the FIRE Arctic Clouds Experiment, J. Geophys. Res., 106(D14), 15015–15028, 2001.

Spracklen, D. V, Pringle, K. J., Carslaw, K. S., Chipperfield, M. P. and Mann, G. W.: A global off-line model of size-resolved aerosol microphysics: I. Model development and prediction of aerosol properties, Atmos. Chem. Phys., 5, 2227–2252, 2005a.

Spracklen, D. V, Pringle, K. J., Carslaw, K. S., Chipperfield, M. P. and Mann, G. W.: A global off-line model of size-resolved aerosol microphysics: II. Identification of key uncertainties, Atmos. Chem. Phys., 5, 3233–3250, 2005b.

Spracklen, D. V, Carslaw, K. S., Kulmala, M., Kerminen, V. M., Sihto, S. L., Riipinen, I., Merikanto, J., Mann, G. W., Chipperfield, M. P., Wiedensohler, A., Birmili, W. and Lihavainen, H.: Contribution of particle formation to global cloud condensation nuclei concentrations, Geophys. Res. Lett., 35(6), D06808, doi:10.1029/2007GL033038, 2008.

1055 Stevens, R. G. and Pierce, J. R.: The contribution of plume-scale nucleation to global and
1056 regional aerosol and CCN concentrations: evaluation and sensitivity to emissions
1057 changes, Atmos. Chem. Phys. Discuss., 14, 21473-21521, doi:10.5194/acpd-14-21473-
1058 2014, 2014.
1059
1060 Stohl, A., Klimont, Z., Eckhardt, S., Kupiainen, K., Shevchenko, V. P., Kopeikin, V. M.
1061 and Novigatsky, A. N.: Black carbon in the Arctic: the underestimated role of gas flaring
1062 and residential combustion emissions, Atmos. Chem. Phys., 13(17), 8833–8855,
1063 doi:10.5194/acp-13-8833-2013, 2013.

1064 Ström, J., Umegard, J., Torseth, K., Tunved, P., Hansson, H. C., Holmen, K., Wismann,
1065 V., Herber, A., and Konig-Langlo, G.: One year of particle size distribution and aerosol
1066 chemical composition measurements at the Zeppelin Station, Svalbard, March 2000–
1067 March 2001, Phys. Chem. Earth, 28, 1181–1190, doi:10.1016/j.pce.2003.08.058, 2003.

1068
1069 Trivitayanurak, W., Adams, P. J., Spracklen, D., and Carslaw, K. S.: Tropospheric
1070 aerosol microphysics simulation with assimilated meteorology: model description and
1071 intermodel comparison, Atmospheric Chemistry and Physics, 8(12), 3149–3168, 2008.
1072
1073 Tunved, P., Ström, J. and Hansson, H.-C.: An investigation of processes controlling the
1074 evolution of the boundary layer aerosol size distribution properties at the Swedish
1075 background station Aspvreten, Atmos. Chem. Phys. Discuss., 4(4), 4507–4543,
1076 doi:10.5194/acpd-4-4507-2004, 2004.
1077

1078 Tunved, P., Ström, J. and Krejci, R.: Arctic aerosol life cycle: linking aerosol size
1079 distributions observed between 2000 and 2010 with air mass transport and precipitation at
1080 Zeppelin station, Ny-Ålesund, Svalbard, Atmos. Chem. Phys., 13(7), 3643–3660,
1081 doi:10.5194/acp-13-3643-2013, 2013.
1082
1083 Twomey, S.: Pollution and the Planetary Albedo, Atmos. Environ., 8, 1251–1256, 1974.
1084
1085 Vehkamäki, H., Kulmala, M., Napari, I., Lehtinen, K. E. J., Timmreck, C., Noppel, M.
1086 and Laaksonen, A.: An improved parameterization for sulfuric acid-water nucleation
1087 rates for tropospheric and stratospheric conditions, J. Geophys. Res., 107(D22), 4610–
1088 4622, 2002.
1089
1090 Verheggen, B., Cozic, J., Weingartner, E., Bower, K., Mertes, S., Connolly, P.,
1091 Gallagher, M., Flynn, M., Choularton, T. and Baltensperger, U.: Aerosol partitioning
1092 between the interstitial and the condensed phase in mixed-phase clouds, J. Geophys. Res.,
1093 112(D23), D23202, doi:10.1029/2007JD008714, 2007.
1094
1095 Wang, M. and Penner, J. E.: Aerosol indirect forcing in a global model with particle
1096 nucleation, Atmos. Chem. Phys., 9(1), 239–260, doi:10.5194/acp-9-239-2009, 2009.
1097
1098 Wang, Q., Jacob, D. J., Fisher, J. a., Mao, J., Leibensperger, E. M., Carouge, C. C., Le
1099 Sager, P., Kondo, Y., Jimenez, J. L., Cubison, M. J. and Doherty, S. J.: Sources of
1100 carbonaceous aerosols and deposited black carbon in the Arctic in winter-spring:

implications for radiative forcing, Atmos. Chem. Phys., 11(23), 12453–12473, doi:10.5194/acp-11-12453-2011, 2011.

Wentworth, G. R., Murphy, J. G., Croft, B., Martin, R. V., Pierce, J. R., Cote, J.-S., Courchesne, I., Tremblay, J.-E., Gagnon, J., Thomas, J. L., Sharma, S., Toom-Sauntry, D., Chivulescu, A., Levasseur, M., and Abbatt, J. P. D.: Ammonia in the summertime Arctic marine boundary layer: Sources, sinks and implications, Atmos. Chem. Phys., 16, 1937-1953, doi:10.5194/acp-16-1937-2016, 2016.

Westervelt, D. M., Pierce, J. R., Riipinen, I., Trivitayanurak, W., Hamed, A., Kulmala, M., Laaksonen, A., Decesari, S., and Adams, P. J.: Formation and growth of nucleated particles into cloud condensation nuclei: model-measurement comparison, Atmos. Chem. Phys., 13, 7645–7663, doi:10.5194/acp-13-7645-2013, 2013.

Williams, J., de Reus, M., Krejci, R., Fischer, H. and Ström, J.: Application of the variability-size relationship to atmospheric aerosol studies: estimating aerosol lifetimes and ages, Atmos. Chem. Phys., 2(1), 43–74, doi:10.5194/acpd-2-43-2002, 2002.

Yu, F. and Luo, G.: Simulation of particle size distribution with a global aerosol model: contribution of nucleation to aerosol and CCN number concentrations, Atmos. Chem. Phys. Discuss., 9, 10597–10645, doi:10.5194/acpd-9-10597-2009, 2009.

Yu, F.: A secondary organic aerosol formation model considering successive oxidation aging and kinetic condensation of organic compounds: Global scale implications, Atmos. Chem. Phys., 11, 1083–1099, doi:10.5194/acp-11-1083-2011, 2011.

Figure Captions:

Figure 1: Measured monthly median number distributions from the scanning mobility particle sizer (SMPS) at Alert for 2011-2013 and the differential mobility particle sizer (DMPS) at Mt. Zeppelin for 2011-2013 for particle sizes between 20 nm and 500 nm. Error bars show the 20-80th percentile of the measurements.

Figure 2: Measurement monthly median aerosol effective diameter from SMPS and DMPS at the two high-Arctic sites, Alert (2011-2013) and Mt. Zeppelin (2011-2013), respectively, for particle sizes between 20 nm and 500 nm. Error bars show the 20th and 80th percentiles.

Figure 3: Seasonal median number distributions from SMPS measurements at Alert (2011-2013) and for the GEOS-Chem-TOMAS dry size distribution simulations (described in Table 1). The measurement 20-80th percentile is in grey shading. Simulations are shown in color as indicated by legend.

Figure 4: Seasonal median number distributions from DMPS measurements at Mt. Zeppelin (2011-2013) and for the GEOS-Chem-TOMAS dry size distribution simulations

(described in Table 1). The measurement 20-80th percentile is in grey shading. Simulations are shown in color as indicated by legend.

Figure 5: Monthly median number concentration for aerosols with diameters of 20-500 nm (N20), 80-500 nm (N80), and 200-500 nm (N200), and effective diameter from the 2011-2013 Alert SMPS measurements and for the four GEOS-Chem-TOMAS dry size distribution simulations described in Table 1. The measurement 20-80th percentile is in grey shading. Simulations are shown in color as indicated by legend.

Figure 6: Monthly median number concentration for aerosols with diameters of 20-500 nm (N20), 80-500 nm (N80), and 200-500 nm (N200), and effective diameter from the 2011-2013 Mt. Zeppelin DMPS measurements and for the four GEOS-Chem-TOMAS dry size distribution simulations described in Table 1. The measurement 20-80th percentile is in grey shading. Simulations are shown in color as indicated by legend.

Figure 7: Geographic distribution of the simulated pan-Arctic surface-layer seasonal-mean dry effective diameter [nm] for the NEWSCAV+COAG simulation. The coloured stars indicate the effective diameter from measurements at Alert (SMPS) and Mt. Zeppelin (DMPS).

Figure 8: Monthly and Arctic mean aerosol number process rates for the entire Arctic troposphere (north of 66°N) for simulation NEWSCAV+COAG. Processes considered for each of four size ranges are condensation, coagulation, particle formation, primary

emissions, wet and dry deposition, transport across 66 °N and net regional buildup or loss rates. The aerosol size ranges are nucleation (D_p<10 nm), Aitken (10<D_p<100 nm), accumulation (100<D_p<1000 nm), and coarse (D_p>1000 nm).

Figure 9: Monthly and Arctic mean aerosol number tendency due to transport within each of four vertical layers between 1) 0-1.5 km, 2) 1.5-4 km, 3) 4-10 km, and 4) above 10 km for the simulation NEWSCAV+COAG for the entire troposphere north of 66°N. Summation of the 4 layers for any given month and size range yields the transport tendency shown in Fig.8. Positive values indicate a net northward transport into the Arctic.

Figure 10: Regional and monthly mean aerosol number lifetime with respect to wet deposition for accumulation-mode aerosol number (100<D_p<1000 nm) nd in the altitude bands of 0-1.5 km, and 1.5-4 km for the GEOS-Chem simulation NEWSCAV+COAG.

Figure 11: Monthly- and regional-mean aerosol number process rates for the entire troposphere north of 50°N for simulation NEWSCAV+COAG. Processes considered for each of four size ranges are nucleation, emissions, coagulation, condensation, wet and dry deposition, transport across 66°N and net regional accumulation or loss rates. The aerosol size ranges are nucleation (D_p<10 nm), Aitken (10<D_p<100 nm), accumulation (100<D_p<1000 nm), and coarse (D_p>1000 nm).

Tables:

Table 1: Summary of the simulations conducted for this study.

Simulation Name	Revised Wet Removal	With Interstitial Coagulation	With New-Particle Formation
STD	no	no	yes
NEWSCAV	yes	no	yes
NEWSCAV+COAG	yes	yes	yes
NONUC	yes	no	no

Table 2: Model-measurement fractional bias (Eq. 6) for total number of aerosols with diameters of 20-100 nm and 100-500 nm at Alert (in reference to Fig. 3). Bias values closest to zero for each season are highlighted in red.

Bias	STD	NEWSCAV	NEWSCAV+COAG	NONUC
20-100 nm				
Winter	1.95	3.45	**0.18**	1.47
Spring	0.83	1.12	-0.46	**-0.36**
Summer	-0.58	0.56	**0.23**	-0.92
Fall	0.15	3.53	0.52	**0.07**
100-500nm				
Winter	0.66	0.87	0.40	**0.34**
Spring	0.38	0.30	**-0.01**	-0.40
Summer	0.98	0.21	**0.05**	-0.43
Fall	0.40	1.34	0.78	**0.01**

Table 3: Model-measurement fractional bias (Eq. 6) for total number of aerosols with diameters of 20-100 nm and 100-500 nm at Mt. Zeppelin (in reference to Fig. 4). Bias values closest to zero for each season are highlighted in red.

Bias	STD	NEWSCAV	NEWSCAV+COAG	NONUC
20-100 nm				
Winter	6.73	12.87	**3.17**	5.43
Spring	0.68	1.01	**-0.40**	-0.43
Summer	-0.65	**-0.21**	-0.54	-0.90
Fall	0.34	4.59	1.14	**0.10**
100-500nm				
Winter	3.24	3.42	2.18	**2.09**
Spring	0.96	0.49	**0.19**	-0.22
Summer	0.60	**0.02**	-0.15	-0.61
Fall	1.50	1.63	0.99	**0.12**

Table 4: Model-measurement mean fractional bias and mean fractional error (Eqs. 7 and 8) for N20, N80, N200 and effective diameter at Alert (in reference to Fig. 5). Bias and error values closest to zero for each season are highlighted in red.

	STD	NEWSCAV	NEWSCAV+COAG	NONUC
MFB				
N20	0.22	0.57	**0.06**	-0.53
N80	0.24	0.36	**0.05**	-0.43
N200	0.74	0.24	0.27	**0.17**
Eff. Diam.	0.17	**-0.05**	**0.05**	0.21
MFE				
N20	0.45	0.57	**0.23**	0.80
N80	0.32	0.37	**0.23**	0.60
N200	0.74	0.30	0.30	**0.29**
Eff. Diam.	0.20	0.10	**0.08**	0.22

Table 5: Model-measurement mean fractional bias and mean fractional error (Eqs. 7 and 8) for N20, N80, N200 and effective diameter at Mt. Zeppelin (in reference to Fig. 6). Bias and error values closest to zero for each season are highlighted in red.

	STD	NEWSCAV	NEWSCAV+COAG	NONUC
MFB				
N20	0.46	0.66	0.21	**-0.18**
N80	0.65	0.57	0.31	**-0.11**
N200	0.86	0.20	0.22	**0.12**
Eff. Diam.	**0.04**	-0.17	-0.07	0.06
MFE				
N20	0.76	0.86	**0.75**	1.03
N80	**0.68**	0.77	**0.68**	0.88
N200	0.86	0.66	**0.54**	0.56
Eff. Diam.	0.12	0.17	**0.10**	0.17

Figure:

Figure 1: Measured monthly median number distributions from the scanning mobility particle sizer (SMPS) at Alert for 2011-2013 and the differential mobility particle sizer (DMPS) at Mt. Zeppelin for 2011-2013 for particle sizes between 20 nm and 500 nm. Error bars show the 20-80th percentile of the measurements.

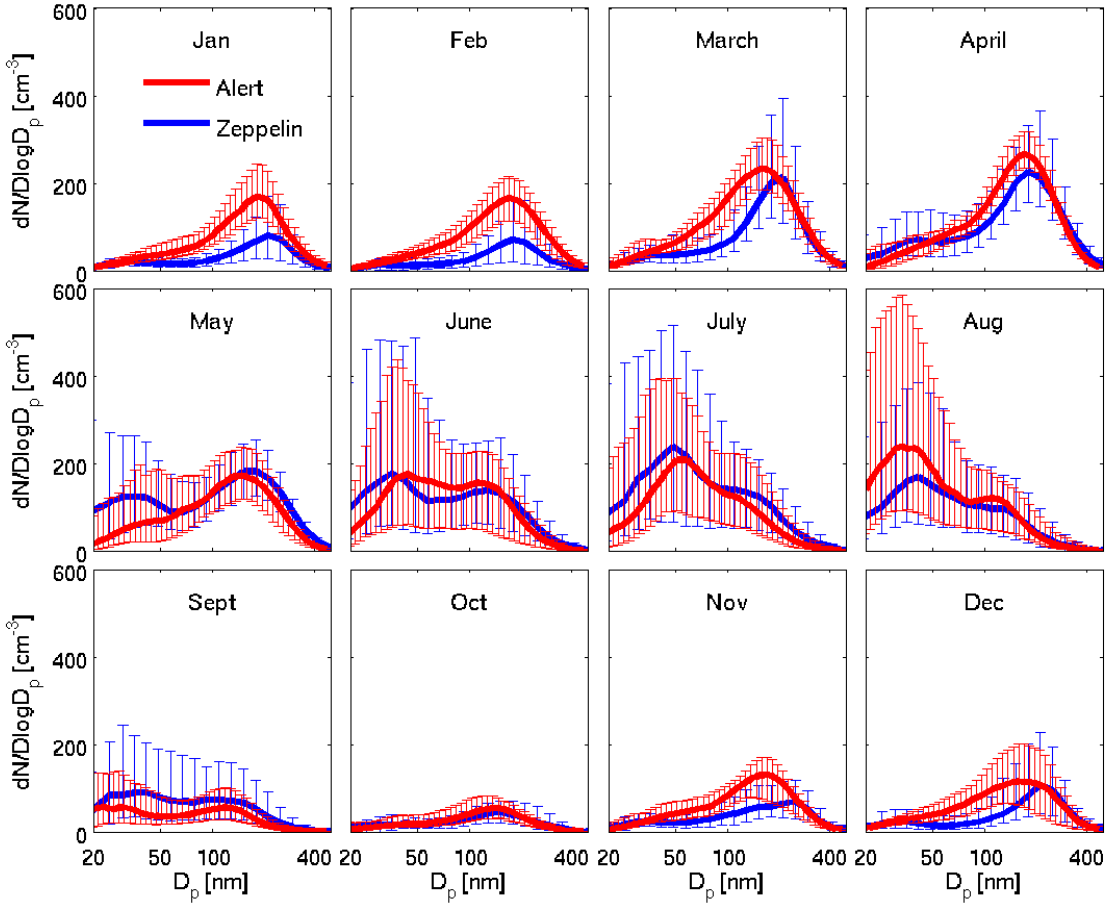

Figure 2: Measurement monthly median aerosol effective diameter from SMPS and DMPS at the two high-Arctic sites, Alert (2011-2013) and Mt. Zeppelin (2011-2013), respectively, for particle sizes between 20 nm and 500 nm. Error bars show the 20th and 80th percentiles.

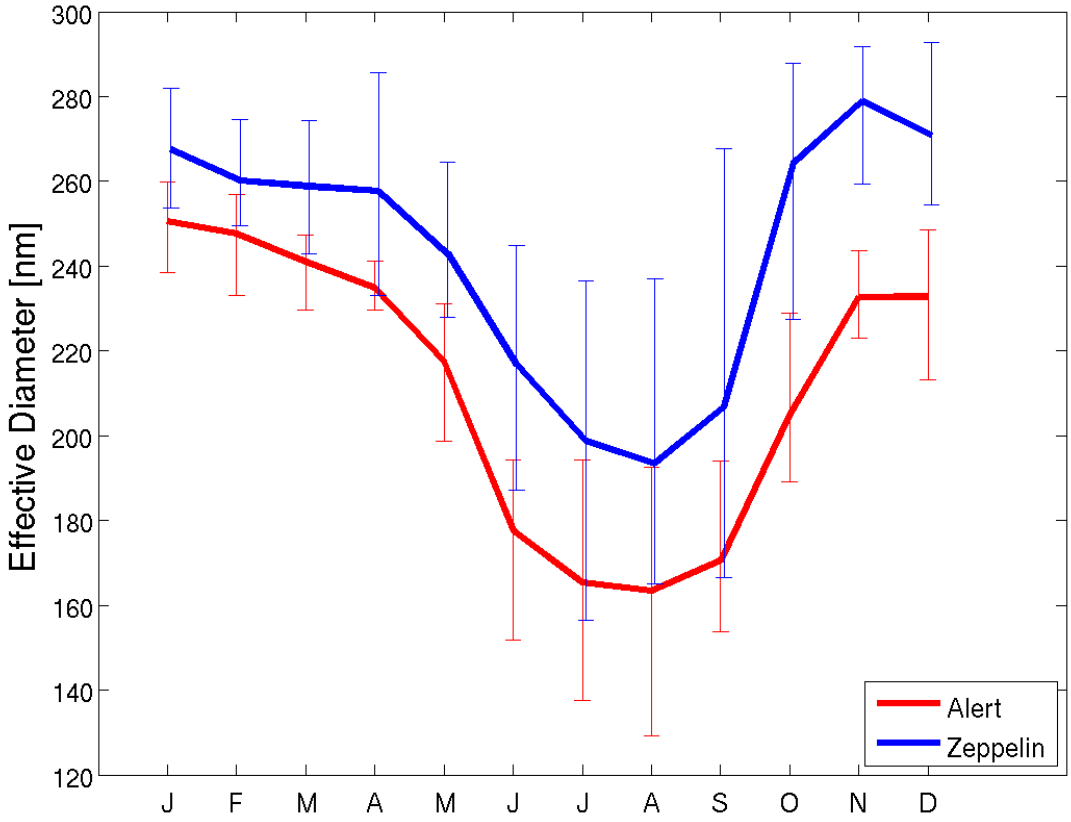

Figure 3: Seasonal median number distributions from SMPS measurements at Alert (2011-2013) and for the GEOS-Chem-TOMAS dry size distribution simulations (described in Table 1). The measurement 20-80th percentile is in grey shading. Simulations are shown in color as indicated by legend.

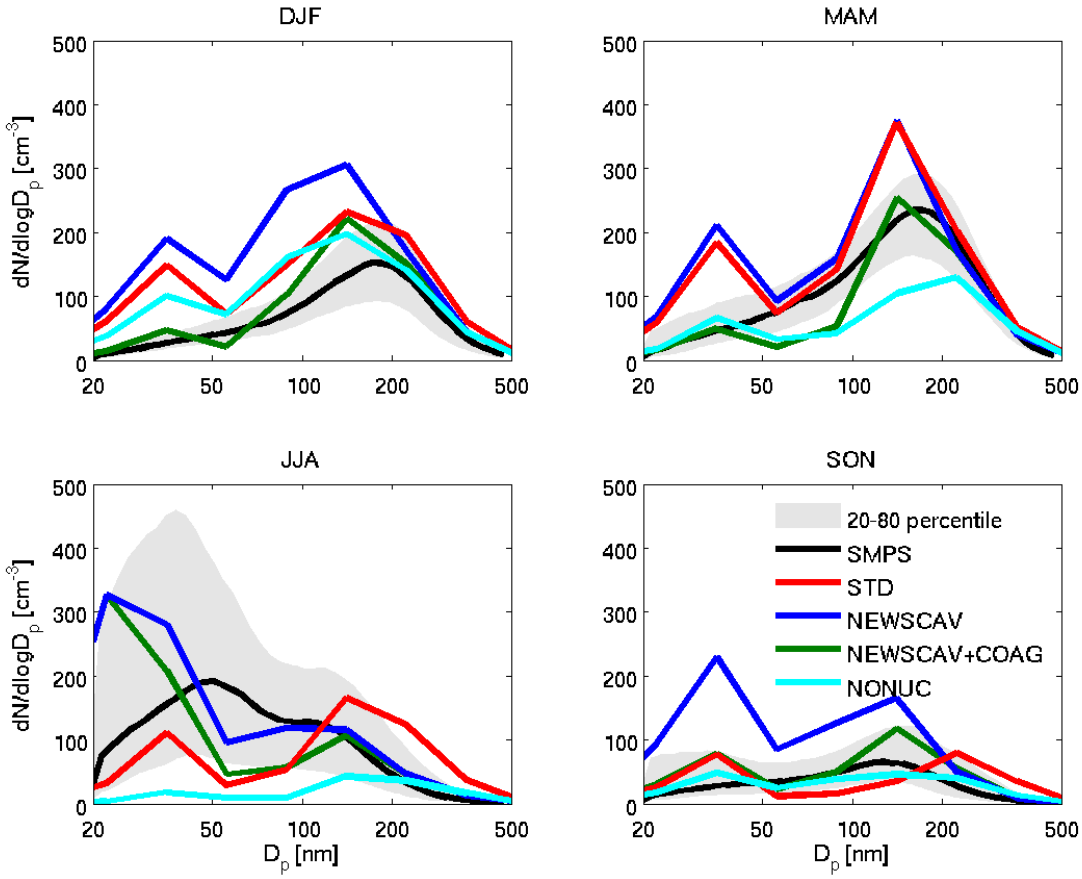

Figure 4: Seasonal median number distributions from DMPS measurements at Mt. Zeppelin (2011-2013) and for the GEOS-Chem-TOMAS dry size distribution simulations (described in Table 1). The measurement 20-80th percentile is in grey shading. Simulations are shown in color as indicated by legend.

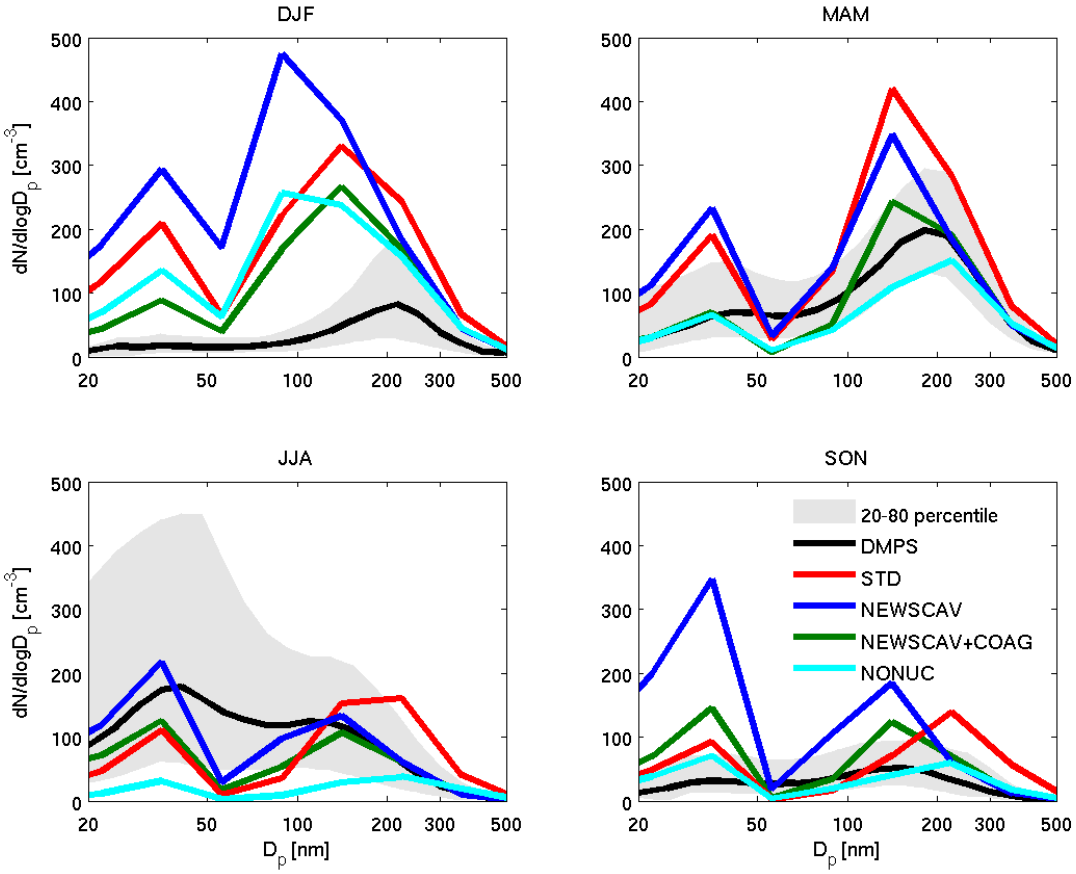

Figure 5: Monthly median number concentration for aerosols with diameters of 20-500 nm (N20), 80-500 nm (N80), and 200-500 nm (N200), and effective diameter from the 2011-2013 Alert SMPS measurements and for the four GEOS-Chem-TOMAS dry size distribution simulations described in Table 1. The measurement 20-80th percentile is in grey shading. Simulations are shown in color as indicated by legend.

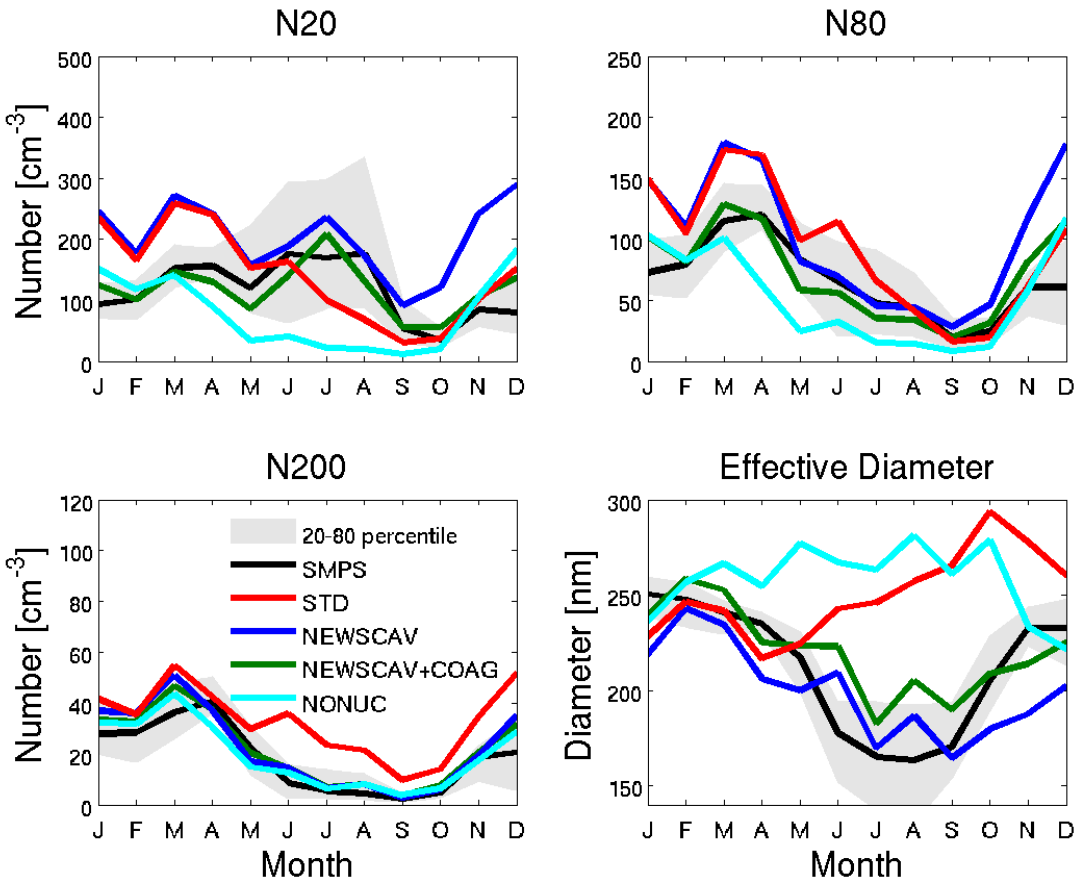

Figure 6: Monthly median number concentration for aerosols with diameters of 20-500 nm (N20), 80-500 nm (N80), and 200-500 nm (N200), and effective diameter from the 2011-2013 Mt. Zeppelin DMPS measurements and for the four GEOS-Chem-TOMAS dry size distribution simulations described in Table 1. The measurement 20-80th percentile is in grey shading. Simulations are shown in color as indicated by legend.

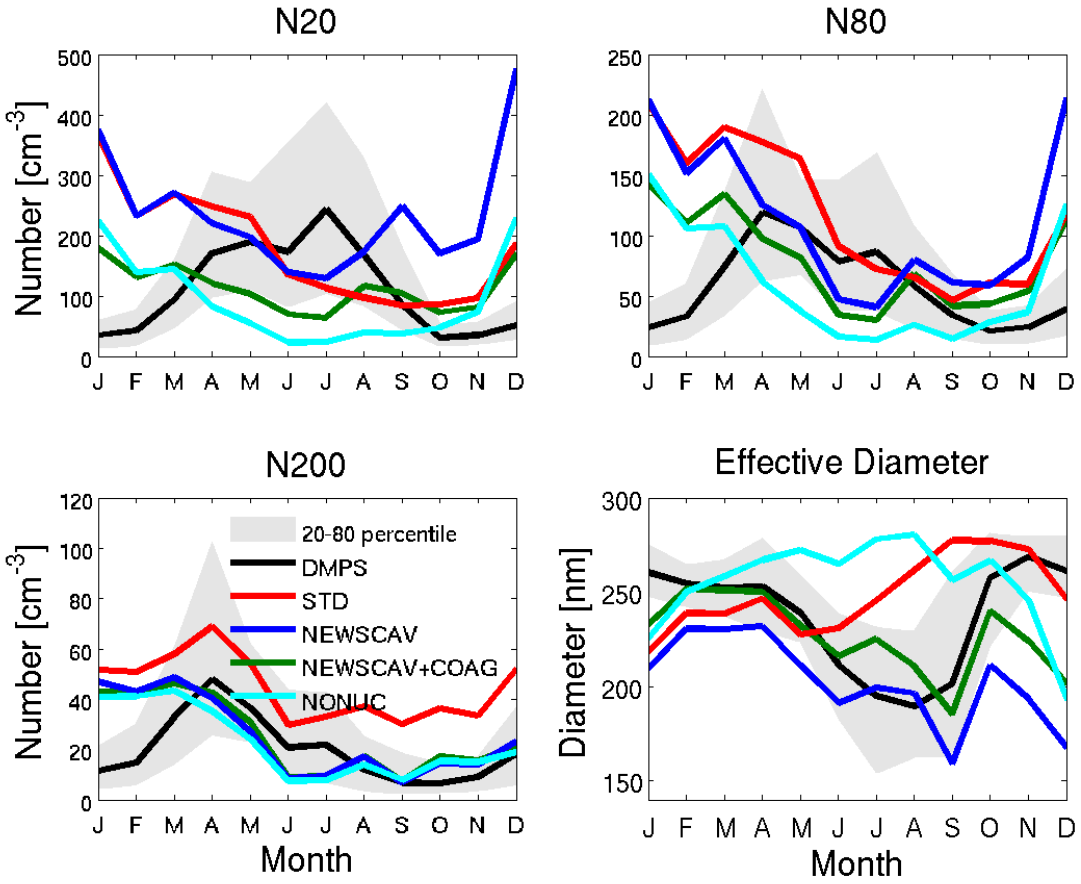

Figure 7: Geographic distribution of the simulated pan-Arctic surface-layer seasonal-mean dry effective diameter [nm] for the NEWSCAV+COAG simulation. The colored stars indicate the effective diameter from measurements at Alert (SMPS) and Mt. Zeppelin (DMPS).

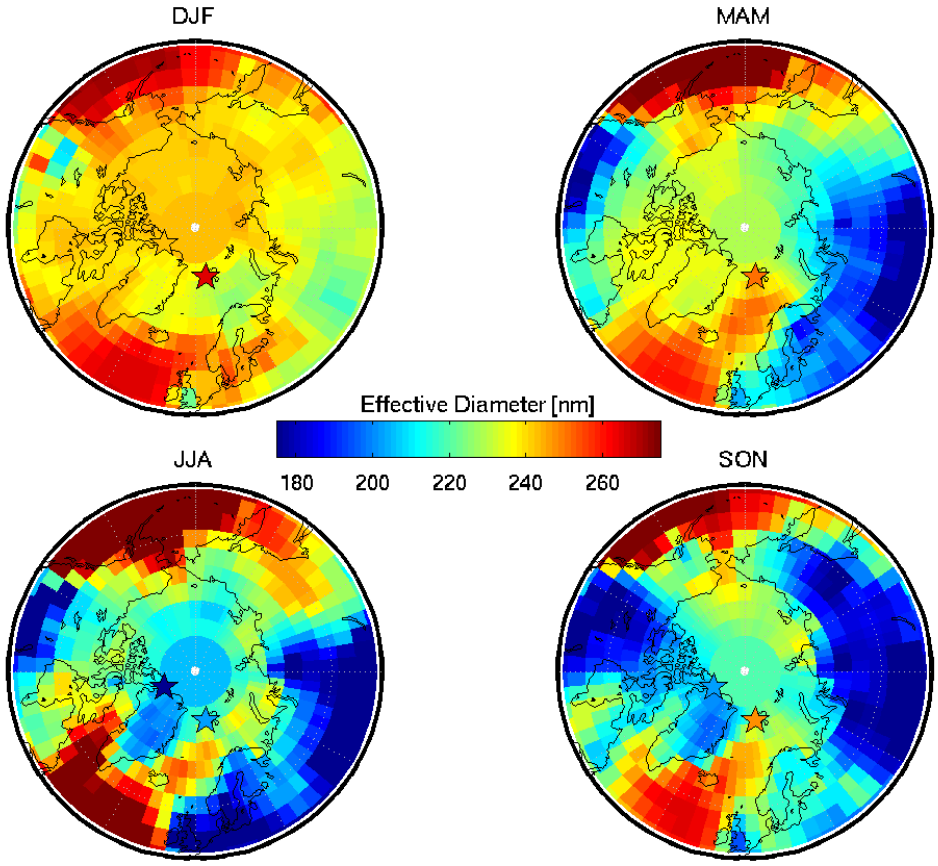

Figure 8: Monthly and Arctic mean aerosol number process rates for the entire Arctic troposphere (north of 66°N) for simulation NEWSCAV+COAG. Processes considered for each of four size ranges are condensation, coagulation, particle formation, primary emissions, wet and dry deposition, transport across 66 °N and net regional buildup or loss rates. The aerosol size ranges are nucleation (D_p<10 nm), Aitken (10<D_p<100 nm), accumulation (100<D_p<1000 nm), and coarse (D_p>1000 nm).

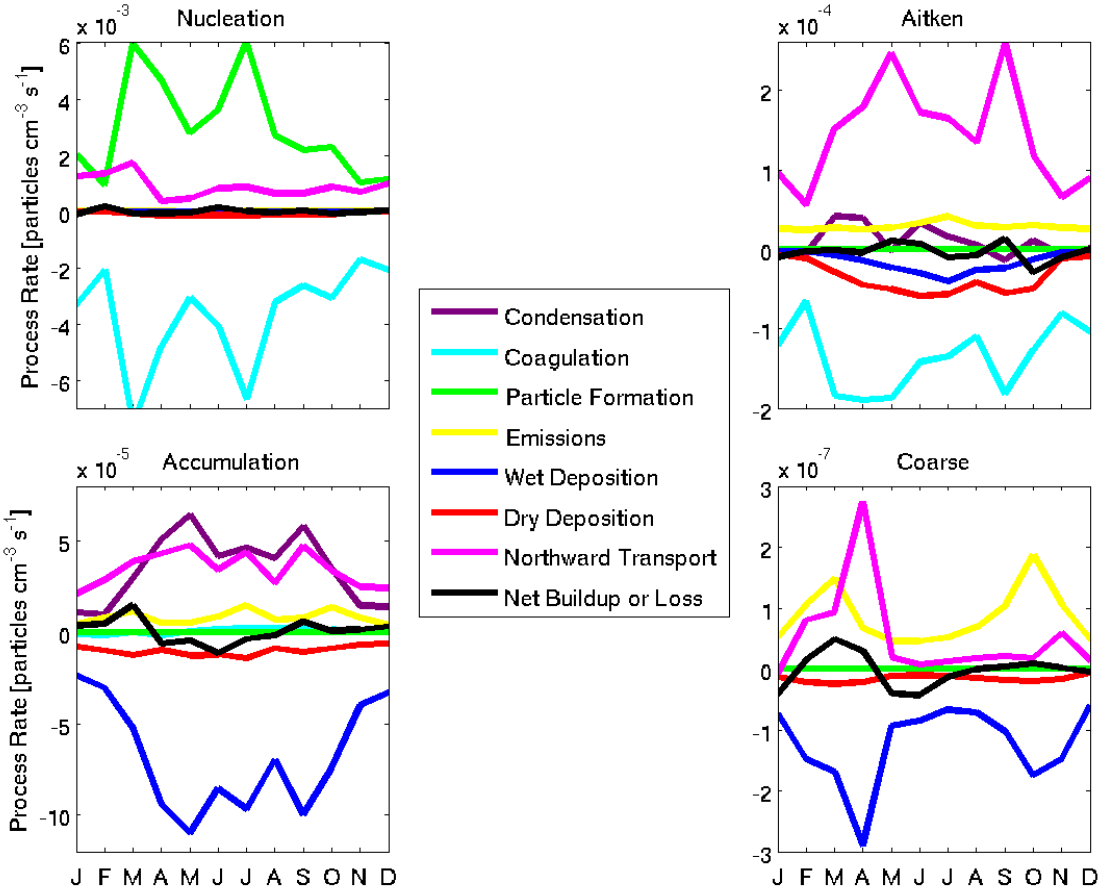

Figure 9: Monthly and Arctic mean aerosol number tendency due to transport within each of four vertical layers between 1) 0-1.5 km, 2) 1.5-4 km, 3) 4-10 km, and 4) above 10 km for the simulation NEWSCAV+COAG for the entire troposphere north of 66°N. Summation of the 4 layers for any given month and size range yields the transport tendency shown in Fig.8. Positive values indicate a net northward transport into the Arctic.

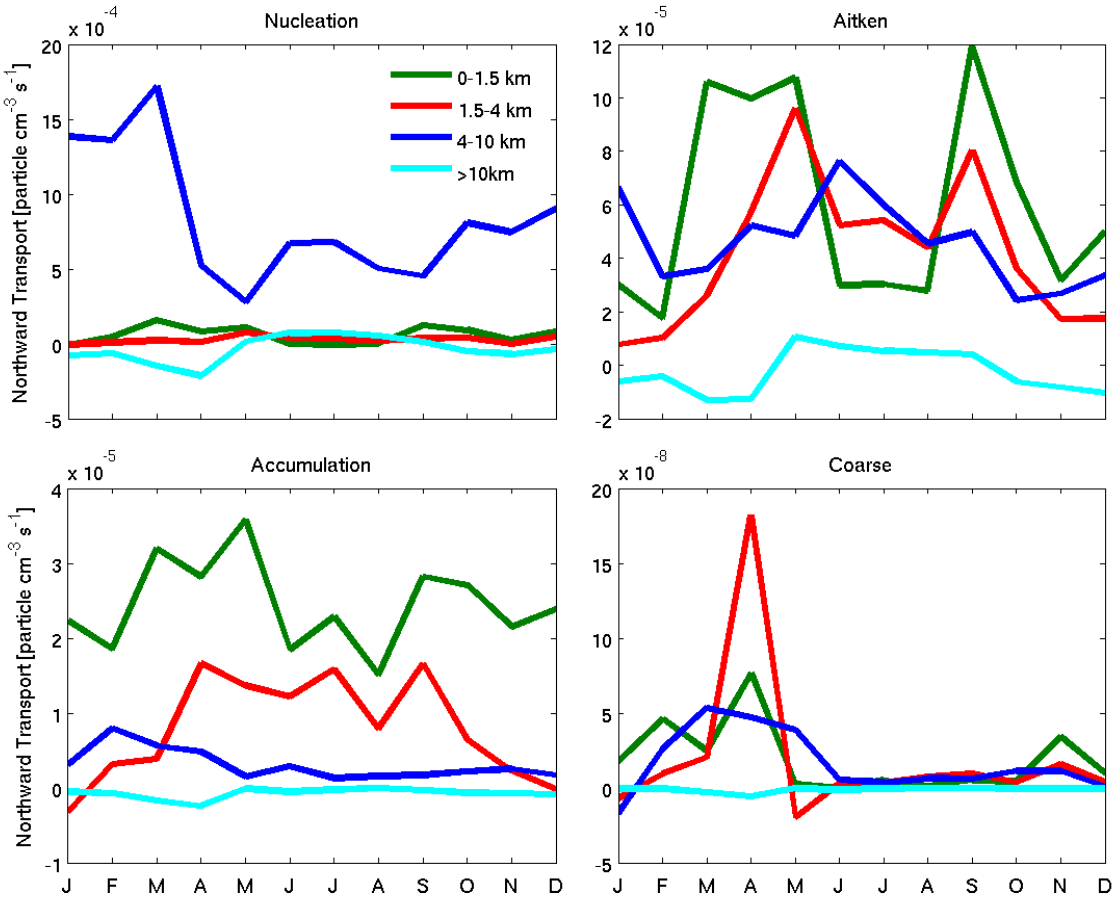

1373

1374

1375 Figure 10: Regional and monthly mean aerosol number lifetime with respect to wet
1376 deposition for accumulation-mode aerosol number ($100<D_p<1000$ nm) in the altitude
1377 bands of 0-1.5 km, and 1.5-4 km for the GEOS-Chem simulation NEWSCAV+COAG.

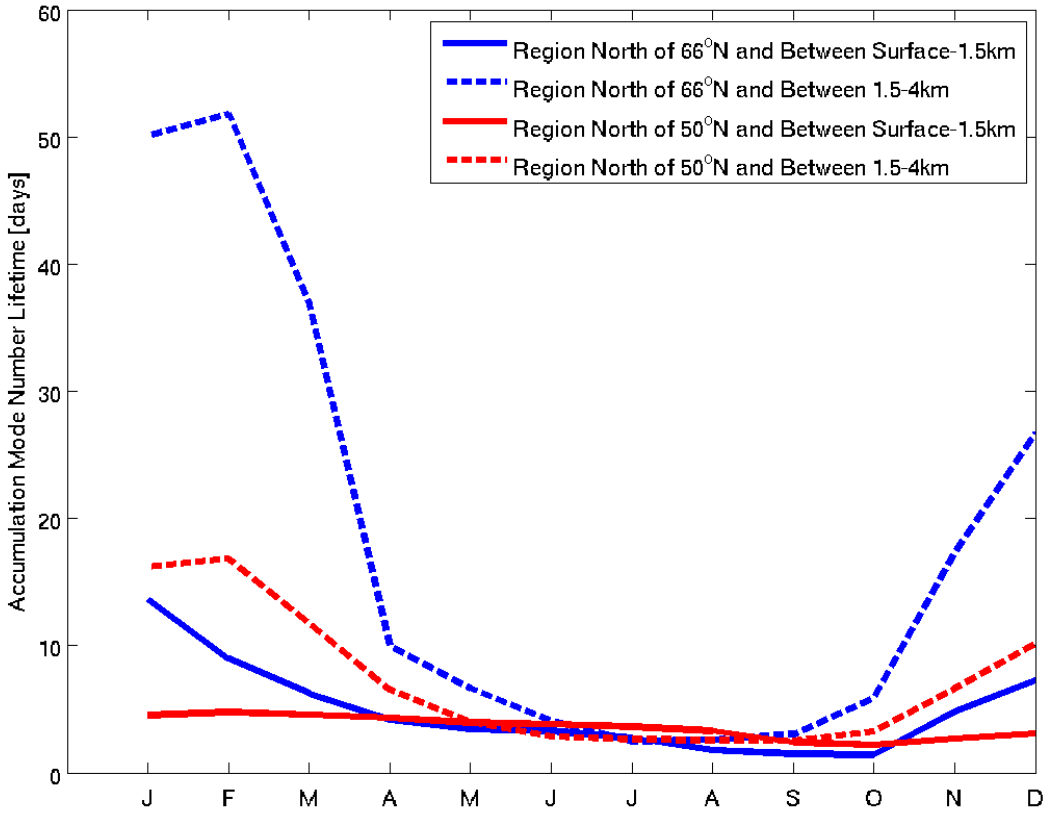

1378
1379

1380

1381

1382

1383

1384

1385

1386

1387 Figure 11: Monthly and Arctic mean aerosol number process rates for the entire
1388 troposphere north of 50°N for simulation NEWSCAV+COAG. Processes considered for
1389 each of four size ranges are nucleation, emissions, coagulation, condensation, wet and dry
1390 deposition, transport across 66°N and net regional accumulation or loss rates. The aerosol
1391 size ranges are nucleation (D_p<10 nm), Aitken (10<D_p<100 nm), accumulation
1392 (100<D_p<1000 nm), and coarse (D_p>1000 nm).

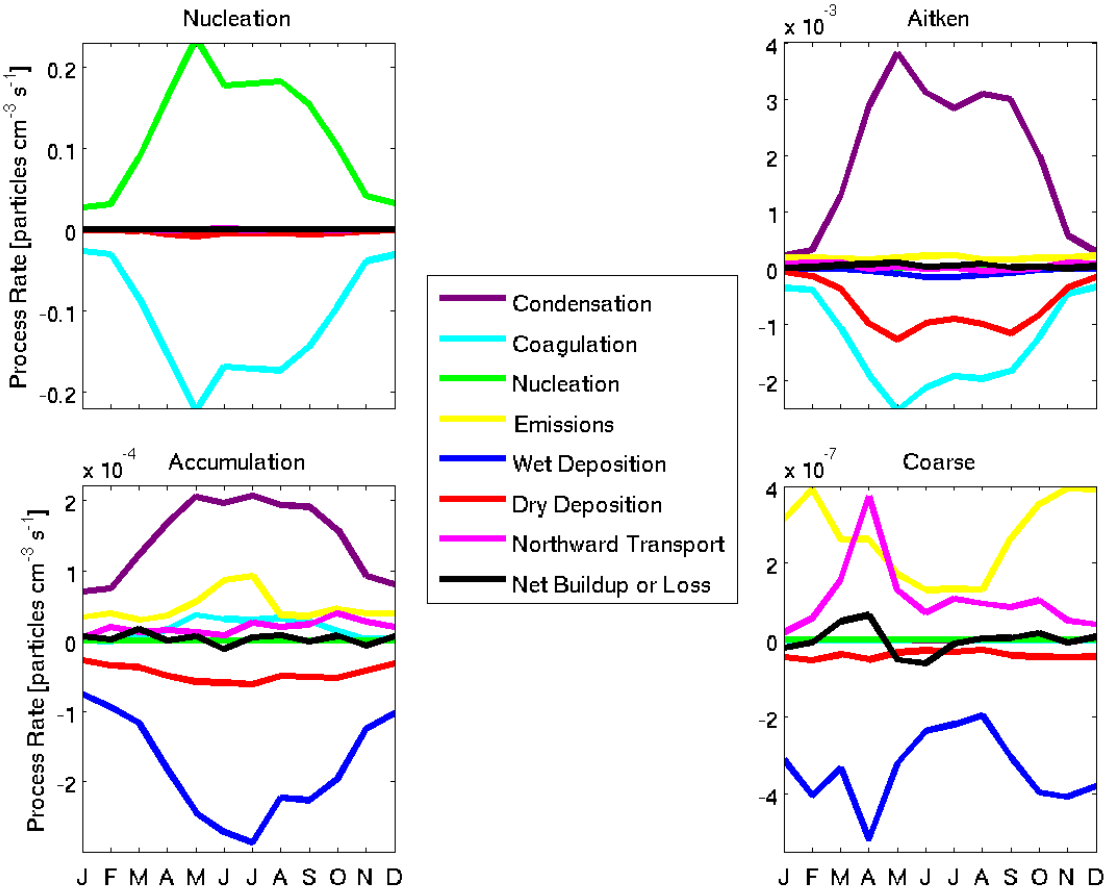

1393